ADVERTIMENT. L'accés als continguts d'aquesta tesi queda condicionat a l'acceptació de les condicions d'ús establertes per la següent llicència Creative Commons: 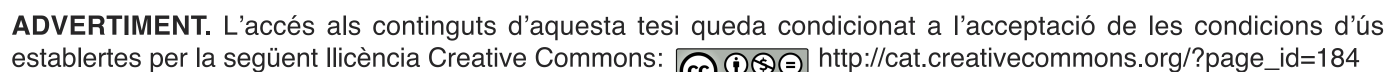 http://cat.creativecommons.org/?page_id=184

ADVERTENCIA. El acceso a los contenidos de esta tesis queda condicionado a la aceptación de las condiciones de uso establecidas por la siguiente licencia Creative Commons: http://es.creativecommons.org/blog/licencias/

WARNING. The access to the contents of this doctoral thesis it is limited to the acceptance of the use conditions set by the following Creative Commons license: 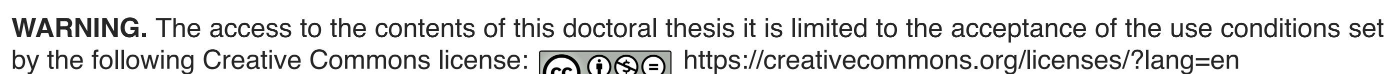 https://creativecommons.org/licenses/?lang=en

Directed self-assembly of block copolymers on chemically nano-patterned surfaces

Memòria presentada per optar al títol de Doctor en Ciència de Materials

Departament de Química

Universitat Autònoma de Barcelona

Laura Evangelio Araujo

DIRECTORS

Francesc Pérez Murano

Institut de Microelectrònica de Barcelona (IMB-CNM, CSIC)

Jordi Fraxedas Calduch

Institut Català de Nanociència i Nanotecnologia (ICN2)

TUTOR

Joan Bausells Roigé

Institut de Microelectrònica de Barcelona (IMB-CNM, CSIC)

2017

Memòria presentada per aspirar al Grau de Doctor per **Laura Evangelio Araujo**

Vist i plau dels directors **Prof. Francesc Pérez Murano** i **Dr. Jordi Fraxedas Calduch**, i tutor **Prof. Joan Bausells Roigé**

Director	Director	Tutor
Francesc Pérez Murano	**Jordi Fraxedas Calduch**	**Joan Bausells Roigé**

Autor

Laura Evangelio Araujo

Bellaterra, 31 de març de 2017

Acknowledgements

"Caminante son tus huellas, el camino y nada más;
Caminante no hay camino, se hace camino al andar.
Al andar se hace el camino, y al volver la vista atrás,
se ve la senda que nunca se ha de volver a pisar.
Caminante no hay camino, sino estelas en la mar"

Antonio Machado (1875-1939)

El meu camí durant la realització de la tesi, no m'ha suposat únicament un canvi professional i científic molt enriquidor, sinó que també m'ha permès conèixer gent que ha marcat d'alguna manera el camí que vaig decidir iniciar fa uns anys. És per això que vull dedicar-vos unes línies d'aquesta memòria.

En primer lloc, m'agradaria agrair els meus director de tesi, Prof. Francesc Pérez Murano i Dr. Jordi Fraxedas Calduch, per haver-me donat l'oportunitat de començar la meva tesi, i haver pogut conèixer el fabulós i curiós món de la nanotecnologia. A en Francesc, m'agradaria agrair-li el seu esforç, suport, consells i dedicació durant tot aquest període, així com la gran quantitat de coses que he anant aprenent d'ell. Gràcies també, Jordi, per haver-me ensenyat a valorar els "petits" detalls de les coses, però sobretot per la teva dedicació en la feina.

M'agradaria agrair també a tots els membres del grup NanoNEMS, no únicament per les nostres discussions científiques, sinó per tots els nostres bons moments. En primer lloc, agrair el suport del meu tutor de tesi Prof. Joan Bausells Roigé. En segon lloc, gràcies als que ja esteu fent els vostres camins fora, però que quan vaig començar em vau ajudar a començar a construir el que avui acabo: Marc, Jordi, Nerea, Giordano, Jordi, Ygezu, Sophie i Nil. I en especial als meus companys de "cafè, ciència i dinar dels divendres": Olga, Gemma, Albert, Matteo, Steven, Angelos i Federico.

No me olvido de vosotras, Ana y Marta, que sé que una ya lo estará echando a faltar. Gracias, Ani, por mostrarme siempre tu amistad, apoyo, fuerza y tus consejos. Empezamos esto juntas, y nos falta muy poquito para terminarlo. Y te agradezco a ti en especial Marti, porque no sólo me enseñaste y dejaste que volara en este camino de copolímeros de bloque, sino que también me has ayudado y aconsejado en el camino de la ciencia y la amistad, y eso se merece más que un *Science* o un *Nature*!

M'agradaria agrair també totes les persones que han fet possible tota la meva feina dins de Sala Blanca i a administració, perquè sempre han estat disposats a ajudar-me quan ho he necessitat; per tant part d'aquesta feina també és vostra. En especial al nanocientífics del Nanolab: Liber, Xevi, Ana i Albert, per ensenyar-me i donar-me suport sempre que ho he necessitat. També moltes gràcies a tota la resta d'àrees de Sala Blanca i administració,

perquè sense vosaltres el nostre treball no seria possible: Marta Gerbolés, Marta Duch, Roser, Carles, Elena, Jose, Annabel, Anna, Nieves...

Tampoco quiero dejar de lado a mi grupo de "gordis", porque si no me van a pedir un pastel como recompensa (aunque sé que me lo pediréis igual…). Muchas gracias a todos, por todos los buenos momentos que hemos pasado en nuestros momentos de desconexión al medio día, y las grandes vivencias que hemos pasado: Sara, Liber, Maria, Sergi, Jordi i Carolina. Sarita, cuantas cosas hemos aprendido juntas eh? Gracias por nuestras largas conversaciones de soporte mañaneras y por nuestras aventuras en el coche ;)

I also want to acknowledge all the project partners I have had the opportunity to work with. Especially all the partners from CoLiSA and PLACYD projects, for having guided and encouraged me in every step of my thesis way. I have learned a lot from all of you. I would like to especially thank my supervisors, Dr. Raluca Tiron and Dr. Stefano Cabrini, during my research stays at CEA-Leti in Grenoble, and at the Molecular Foundry in Berkeley, for their support and for giving me the opportunity to work with them in a remarkable working environment. Thanks to that, I have had the chance of not only exchange knowledge with scientists from all around the world, but also to meet incredible people. Un grand merci à Maxime, Ahmed, Gaëlle et Guillaume pour leur aide et leur accueil. And thank you Alison, Hilary, Tony, Félix and Maria Elena, to share with me and make even more incredible the three months I spent in California.

También me gustaría agradecer a todos los colaboradores con los que he podido trabajar durante este último periodo de tiempo. Gracias a Tiberio, Mari Cruz, Aurora y Edgar, por enseñarme e iniciarme en el mundo del GISAXS.

Fuera del ámbito científico, y no por ello menos importante, me gustaría agradecer a todas las personas que me han ayudado, animado y compartido conmigo grandes momentos en estos años de tesis, pero sobretodo en esta última recta final: Pili, Paco, Laura, Natàlia, Carlos, Tat, Fran, Marta, Jordi, Ismi, Anna i Miriam.

El especial agradecimiento os lo debo a vosotros, mis padres y hermano, porque siempre me habéis ayudado y apoyado en todas mis decisiones. Vosotros me animasteis a empezar mi camino, a aprender a levantarme y continuar en él hasta el final. Por eso, gracias en esto, y en todos los aspectos de mi vida.

Y por último a ti, Javi, porque decidiste iniciar y recorrer nuestro camino en la vida juntos. Gracias por todo el apoyo que me has dado durante estos años, y en especial por la infinita paciencia que has demostrado siempre, tu amabilidad y cariño.

Gràcies a tots, perquè tots formeu part d'aquest camí!

This research has been supported by the Ministry of Education of Spain with the FPU grant 13/03746.

Resum

La tesi doctoral titulada *"Auto-assemblatge de copolímers de bloc per modificació química de la superfície"*, presenta com a objectiu principal el desenvolupament, implementació i caracterització d'un mètode de guiatge de copolímers de bloc basat en la modificació química de la superfície. El desenvolupament d'aquest mètode de nanofabricació contribueix a la futura generació de dispositius i circuits nanoelectrònics.

Primer de tot, es presenten els aspectes generals sobre l'auto-assemblatge dirigit de copolímers de bloc, així com el seu rol dins del futur de la nanoelectrònica comparat amb altres tecnologies emergents. Després, per tal d'entendre i determinar les interaccions que tenen lloc durant el procés d'auto-assemblatge, es dóna una visió general sobre els processos químics i físics que tenen lloc en les pel · lícules primes de copolímers de bloc.

La part principal de la tesi es focalitza en l'estudi, desenvolupament i implementació d'un mètode de guiatge químic per tal de dirigir l'auto-assemblatge de copolímers de bloc. A banda d'estudiar el procés experimental, també es caracteritzen els mecanismes que condueixen l'alineament i s'introdueixen a un model per simular el procés d'auto-assemblatge dirigit. A més, també es presenta la transferència del procés a una línia pilot industrial de fabricació de circuits integrats.

La implementació del procés de guiatge químic s'ha provat no únicament amb materials comercials, sinó també amb nous sistemes polimèrics que permeten arribar a mides per sota dels 10 nm. Per aquests sistemes, es defineix un nou mètode de guiatge basat en la combinació de modificacions topogràfiques i químiques.

Per tal d'entendre millor el procés, s'estudien tècniques específiques de metrologia. En particular, mitjançant tècniques d'alta energia de rajos X, es descriuen les principals diferències entre patrons químics de guiatge. D'altra banda, les propietats nanomecàniques dels diferents dominis del copolímer es determinen mitjançant el mode *peak force tapping* de la microscòpia de força atòmica.

Finalment, es mostra un mètode per transferir els motius del copolímer al substrat. Aquest es basa en la infiltració d'un domini del copolímer. La infiltració canvia les propietats del material i el fa més resistiu al gravat amb oxigen. D'altra banda, i com a aplicació final, es presenta un procés de fabricació de ressonadors nanomecànics, basats en el procés d'auto-assemblatge de copolímers de bloc amb infiltració.

Summary

The thesis entitled *"Directed self-assembly of block copolymers on chemically nano-patterned surfaces"*, aboard the challenge of the development, implementation and characterization of a chemical epitaxy process to direct self-assemble block copolymers. The development of this nanofabrication method contributes to the next generation of nanoelectronic devices and circuits.

Firstly, the main aspects of directed self-assembly of block copolymers and its role and status in the future of nanoelectronics is presented, and compared with other powerful technologies. Then, a general overview about the physics and chemistry involved in block copolymer thin films is presented, in order to understand and determine the interactions taking place during the DSA process.

The main part of the thesis is focused on the study, development and implementation of a chemical epitaxy approach to guide the self-assembly of block copolymers. Apart from the process development, the mechanisms which drive the block copolymer alignment are characterized and simulated into a DSA model. Moreover, the process transfer to a more industrial pilot line is presented.

The implementation of the chemical epitaxy process is addressed not only with commercial block copolymers, but also with new polymer systems which allow getting sub- 10 nm resolution. For these systems, a new guiding method is presented based on the combination of a chemical and graphoepitaxy approach.

To better understand the DSA process, dedicated metrology methods are also studied. In particular, by using high-energy X-ray techniques it is possible to describe the main characteristics of the chemical guiding patterns. On the other hand, the nanomechanical properties of block copolymer domains are studied by using the peak force tapping mode in atomic force microscopy.

A reliable method to pattern transfer the block copolymer features into the substrate is showed. It is based on infiltrating one block copolymer domain and enhancing thus, its resistivity to plasma etching. Finally, as a final application, a novel fabrication process of a nanowire mechanical resonator by means of DSA and infiltration is presented.

Contents

Introduction 1

1. Introduction to nanolithography 5

1.1. Introduction 7

1.2. Status and challenges of lithography for microelectronics 8

1.2.1. Optical lithography 9

1.2.2. Extreme ultraviolet lithography 10

1.2.3. Maskless lithography 12

1.2.4. Nanoimprint lithography 18

1.2.5. Directed self-assembly of block copolymers 19

1.3. Summary: lithography status, issues and challenges 21

1.4. References 23

2. Chemistry and physics of block copolymer materials 27

2.1. Block copolymers and their synthesis 29

2.2. Physics of block copolymers 32

2.2.1. Order-disorder transition in block copolymers 32

2.2.2. Morphologies of diblock copolymers 33

2.2.3. Block copolymers in thin films 34

2.2.4. Interface neutralization 37

2.2.5. Thermal and solvent annealing of block copolymer films 37

2.3. Modelling of block copolymer directed self-assembly 39

2.3.1. Block copolymer kinetics 40

2.3.2. Field-theoretic simulations and self-consistent field theory 41

2.4. High-chi block copolymers 42

2.4.1. Organic based high-χ block copolymers 43

2.4.2. Inorganic based high-χ block copolymers 43

2.5. References 45

3. Directed self-assembly of PS-*b*-PMMA BCPs by chemical epitaxy ... 53

3.1. Introduction to DSA of block copolymers by chemical epitaxy ... 55

3.2. Development of chemical epitaxy by substrate functionalization ... 57

3.2.1. Materials and methods ... 57

3.2.2. Directed self-assembly by chemical epitaxy of PS-*b*-PMMA results ... 61

3.3. Characterization of the surface free energy of chemical guiding patterns ... 66

3.3.1. Experimental method to determine the interface interactions for modeling the chemical epitaxy DSA process ... 66

3.3.2. Role of the surface interactions by field-theoretic simulations and self-consistent field theory on chemical epitaxy DSA process ... 73

3.4. Manufacturability of chemical epitaxy by substrate functionalization ... 77

3.4.1. Materials and methods ... 78

3.4.2. Directed self-assembly by chemical epitaxy of PS-*b*-PMMA results ... 83

3.5. Development and implementation of chemical epitaxy by UV substrate functionalization ... 85

3.5.1. Chemical surface characterization of UV exposed surfaces ... 86

3.5.2. Surface free energy characterization ... 90

3.5.3. DSA of chemical epitaxy by UV surface functionalization ... 92

3.6. Chemical epitaxy based resistless direct writing methods ... 94

3.6.1. Introduction ... 94

3.6.2. E-beam lithography direct writing ... 94

3.6.3. Local Anodic Oxidation based AFM nanolithography ... 99

3.6.4. Summary and comparison ... 108

3.7. Summary and conclusions ... 109

3.8. References ... 111

4. Directed self-assembly of PS-*b*PMMA BCPs by graphoepitaxy ... 115

4.1. Introduction to directed self-assembly of block copolymers by graphoepitaxy 117

4.2. Development and implementation of graphoepitaxy on PS-*b*-PMMA by means of e-beam lithography ... 119

4.2.1. Materials and methods ... 119

4.2.2. Directed self-assembly by graphoepitaxy of PS-*b*-PMMA results 122

4.3. Development and implementation of graphoepitaxy on PS-*b*-PMMA by means of photolithography 124

4.3.1. Materials and methods 124

4.3.2. Directed self-assembly by graphoepitaxy results 128

4.4. Surface affinity control on topographical guiding patterns 129

4.5. Summary and conclusions 132

4.6. References 133

5. Directed self-assembly of high-χ block copolymers 137

5.1. Introduction to high-χ block copolymers 139

5.2. PS-*b*-PLA systems 139

5.2.1. PS-*b*-PLA synthesis 139

5.2.2. PS-*b*-PLA self-assembly 140

5.2.3. PS-*b*-PLA directed self-assembly by chemical epitaxy 145

5.2.4. Experimental determination of surface free energy for PS-*b*-PLA DSA... 146

5.3. PLA-*b*-PDMS-*b*-PLA systems 147

5.3.1. PLA-*b*-PDMS-*b*-PLA synthesis 147

5.3.2. PLA-*b*-PDMS-*b*-PLA self-assembly 148

5.3.3. PLA-*b*-PDMS-*b*-PLA directed self-assembly by chemical epitaxy 150

5.3.4. PLA-*b*-PDMS-*b*-PLA directed self-assembly by chemo/grapho epitaxy .. 151

5.4. Summary and conclusions 157

5.5. References 158

6. Characterization of block copolymers and chemical guiding patterns using synchrotron radiation 161

6.1. Chemical guiding pattern characterization by X-Ray photoemission 163

6.1.1. Characterization of chemical guiding patterns created by electron beam lithography and oxygen plasma functionalization 166

6.1.2. Characterization of guiding patterns by direct writing techniques 169

6.2. Block copolymer morphology and self-assembly characterization by GISAXS 172

6.2.1. Basis of grazing incidence X-ray technique 172

6.2.2. Block copolymer self-assembly GISAXS characterization 174

6.2.3. Static GISAXS studies on block copolymer films 175

6.3. Summary and conclusions... 179

6.4. References 180

7. Pattern transfer of block copolymers and application in device fabrication.. 183

7.1. Conventional atomic layer deposition 185

7.1.1. Introduction 185

7.1.2. Use of atomic layer deposition for block copolymer pattern transfer....... 187

7.2. Sequential Infiltration Synthesis.. 190

7.2.1. Introduction 190

7.2.2. Use of sequential infiltration synthesis for pattern transfer 190

7.3. Local nanomechanical properties of PS-*b*-PMMA self-assembly 194

7.3.1. Introduction 194

7.3.2. Optimal Indentation Conditions 195

7.3.3. Characterization of PS-*b*-PMMA thin films 196

7.3.4. Characterization PS-*b*-PMMA thin films after atomic layer deposition... 197

7.3.5. Characterization of PS-*b*-PMMA after sequential infiltration synthesis .. 199

7.4. Fabrication of nanomechanical devices based on metallic oxide nanowires..... 201

7.4.1. Materials and methods.. 201

7.4.2. Nanomechanical resonators fabrication results 207

7.5. Summary and conclusions... 210

7.6. References 211

General conclusions.. 215

Conclusions generals 219

Annexes.. 223

Annex I. Acronyms List... 225

Annex 2. Scientific contributions... 229

Introduction

The term *´nano´* means the billionth part of something, and thus *nanoscience* refers to the study of phenomena taking place in materials at atomic, molecular and macromolecular scales, where matter properties differ significantly from those at larger scale. It is a multidisciplinary science which is based on the convergence of a mix of scientific and technological domains. Its application to different techniques which allow the manipulation, fabrication and characterization of matter with an industrial objective is referred as *nanotechnology*.

The conceptual foundations of *nanotechnology* were partially inspired by the physicist *Richard Feynman*, Nobel Prize winner for Physics in 1965, during a conference of the American Physical Society in 1959. It was entitled *´There is plenty of room at the bottom´*, and he discussed the importance of manipulating and controlling things at the nanometer scale, and how they could tell us about the peculiar phenomena that occur in complex situations.

Nanofabrication is one aspect of nanotechnology that has developed from the evolution of microelectronics during the last decades on one side, and on the other side, from the incorporation of novel methods and techniques from nanoscience. Since the invention of the integrated circuit more than half a century ago, there has been an exponential growth in the number of transistors per chip and an associated decrease in the smallest width. Lithography is the central process in nanofabrication, and its tremendous technological evolution, in particular for what it concerns optical lithography, has delivered the possibility to define nanoscale patterns at high throughput and reproducibility. However, the current technological limits will soon be reached, and emerging technologies will take over.

It is in the framework of the need of new patterning methods for nanoelectronics that the present thesis arises. The initial overall objective of thesis has been the research of novel solutions for nanolithography, a topic of interest for the two research centers where the work has been developed (*IMB-CNM-CSIC*, and *ICN2*) and also for the European research community, as exemplified by the European projects where it has contributed. Actually, the work of this thesis has been, in several aspects, dictated by the involvement mainly in the CoLiSA Project (*Computational Lithography for directed self-assembly: Materials, Models and Processes - FP7-619793*) but also in SNM (*Single Nanometer Manufacturing for beyond CMOS devices - FP7-318804*) and PLACYD (*Pilot Line for Self-Assembly Copolymers Delivery - ENICAC JU-621217*) projects.

D*irected self-assembly (DSA) of block copolymers (BCPs)*, offers very attractive characteristics from an industrial point of view: high resolution, low cost and high throughput. The ability of BCPs to self-assemble at the nanoscale makes them of interest to use as complementary solution to conventional lithographic techniques. Therefore, they are being to be exploited to form small features at low cost processing. DSA integrates *bottom-up* self-assembly with *top-down* conventional lithography responsible to direct the orientation of the BCPs. There are basically two approaches to do so: *graphoepitaxy* which uses topographical features of lithographically patterned surfaces, and *chemical epitaxy* which employs dense chemical patterns created normally on a polymeric surface.

The research reported in this thesis, concerns the overall objective of study, development, characterization and optimization of a chemical epitaxy approach to direct self-assemble BCPs for nanoelectronic applications. The outline of the thesis is divided in seven chapters, and they cover different aspects of BCPs, from the basic concepts to the application of DSA on the fabrication of a nanomechanical resonator.

The first chapter aims to give a general overview of the conventional and next generation lithography techniques, and bring together the foremost advances and challenges for the next generation logic node. It also describes which the main aspects of DSA are, and its role and status in the future of microelectronics industry.

On the other hand, in order to determine the mechanisms involved during the DSA process, an understanding of the basic concepts of BCPs is of great importance. Therefore, *chapter 2* is focused on the study of BCP physics from its bulk state to thin films.

The study, development and implantation of different chemical epitaxy processes are discussed in *chapter 3,* which covers the central part of the thesis work. This chapter, apart from giving a summary of the experimental methods and results, leads down the whole chemical characterization performed to understand the interactions which take place between the surface and the BCP domains. Furthermore, a novel experimental method which allows predicting the chemical affinities is presented. With the obtained data it has been possible to simulate and predict the DSA process by using self-consistent mean-field calculations. On the other hand, the process transfer to a more industrial focused pilot line in *CEA-Leti*, is presented.

In *chapter 4*, the implementation of graphoepitaxy process by means of photolithography, is presented. The BCP orientation is controlled by the tuning of experimental conditions and materials used. On the other side, the topographical guiding pattern designs and the subsequent DSA process are focused on the fabrication of a nanomechanical resonator presented in *chapter 7*.

In order to demonstrate the DSA implemented processes for smaller structures, the self-assembly behavior of materials which offer smaller features than the most used BCP, *poly(styrene-b-methacrylate),* (PS-*b*-PMMA), is presented. Both, chemical and graphoepitaxy approaches, are implemented for the DSA of this new materials. These methods are explained in *chapter 5*.

The better understanding and characterization of DSA deserves dedicated metrology methods. In general, the improvement in nanofabrication methods allowing to produce sub-10 nm features has trigger a lot on activity to develop adapted characterization tools. In particular, high-energy X-ray techniques are capable to give information about the chemical nature of guiding patterns. Therefore, *chapter 6* describes the main differences between chemical guiding patterns created in different ways, by using X-ray techniques based on synchrotron radiation. On the other hand, the characterization of BCP pitch and shapes is corroborated by grazing incidence small-angle scattering (GISAXS). Besides of providing information about BCP morphology, this technique allows to perform in-situ analysis and give a general overview of the self-assembly mechanisms at early stages.

To take advantage of BCP DSA, an accurate pattern transfer to the substrate is needed. However, the poor contrast between most part of the polymers requires the use of alternative methods to enhance the etch resistivity of one of the blocks. *Chapter 7* demonstrates the use of sequential infiltration synthesis (SIS) to pattern transfer the BCP features. Moreover, it is described a novel fabrication process of a nanowire mechanical resonator based on the combination of DSA and SIS.

Chapter 1

Introduction to nanolithography

For many decades, Moore's Law has delivered to the microelectronic industry more functionality while decreasing production costs. However, this continuous tendency to reduce the dimensions of a device forcedly implies new challenges, hence new fabrication strategies need to be considered.

Nowadays, extreme ultraviolet lithography (EUV) using 13.5 nm wavelengths, is the leading candidate to succeed 193 nm immersion lithography for the next generation logic nodes. Nevertheless, EUV is still not fully developed, and other approaches, like directed self-assembly or nanoimprint are much closer to manufacturing implementation than they used to be.

This chapter gives an overview of the different state-of-the-art lithography techniques and their status, challenges and possible driving forces for implementation.

1.1. Introduction

For many decades, many areas of science and technology are demanding the continuous resolution improvement of patterning methods. A prominent example is the semiconductor industry, where the increase of density in integrated circuits requires reducing the critical dimensions of the transistors, as dictated by *Moore*'s Law.[1] This law describes the exponential growth in complexity of integrated circuits, and it is based on the observation that the number of transistors in a dense integrated circuit (IC) was doubling every two years. In 1975, it was adjusted to a doubling every year and a half.[2]

For many years, the scaling has consisted in only reducing the feature size, and thus has resulted in a rapid progress in terms of functionality and cost-effectiveness. This has meant that every two years, devices have become more powerful, smaller and cheaper. Nevertheless, this exponential growth is approaching physical limits, and transistors are getting too small to actually manufacture efficiently.

In the early 2000s, it was realized that chips began to become too hot during operation. Therefore, manufacturers had to redesign the IC, so that each chip contained not only one processor, but more. It enabled microelectronics industry to continue shrinking the IC size and follow *Moore*'s path. Nevertheless, there is still unknown what will happen in the next years, when scaling will be no longer available due to quantum effects leading to interferences and coupling between paths.

The international technology roadmap for semiconductors (ITRS) is a document produced by semiconductor experts with the aim to enable equipment and materials suppliers to know about the future requirements. According to the ITRS, there are two directions for further progress in the microelectronics industry. The first trend is called *More Moore*, and it is based on the continuous miniaturization, but reinforced by the incorporation of new materials and processes. On the other hand, the second direction is called *More than Moore*, and it is characterized by the addition of non-digital functionalities which contribute to the miniaturization of electronic systems, although not at the same rate. *More than Moore* technologies do not represent an alternative, but an integration of digital and non-digital functionalities which can be used in a very extensive list of application fields (chemical sensors, smart cities, self-driving cars…), which do not require an extreme scaling demand.

Therefore, microelectronics does not only need to provide performance on its traditional market, but also to develop new markets, based on non-electronic functions of IC. That is, microelectronics has to be a platform to biological and medical science, in order to develop new applications and capabilities.[3]

1.2. Status and challenges of lithography for microelectronics

Lithography is derived from *Ancient Greek*, *'lithos'* and *'graphia'*, which mean *stone* and *to write*, respectively. It was invented around 1796 in Germany by *Alois Senefelder*. He discovered that he could duplicate his scripts by writing them in grey crayon on slabs of limestone, and then printing them with rolled-on ink. From this seminal discovery to the current lithography processes many efforts in research and development have been dedicated.

In microelectronics, lithography refers to a micro/nano fabrication technique used to make IC, as well as micro and nano electromechanical systems (MEMS and NEMS). It is a highly specialized process used to transfer the patterns from a mask to a layer.

For many technological generations, the scaling of physical dimensions has been enabled by the continuous improvements of optical lithography. It has been achieved thanks to the reduction of the wavelength and/or to the increase of the numerical aperture (NA). Nevertheless, its physical limits are coming closer due to intrinsic limitations in resolution, and alternative non-optical lithography approaches are taking over.

Figure 1.1 shows a graph with the lithography scaling as a function of the time and wafer size. Nowadays, extreme ultraviolet (EUV) lithography seems to be almost ready for high-volume manufacturing, while new technologies like DSA or nanoimprint lithography (NIL) are gaining consensus.

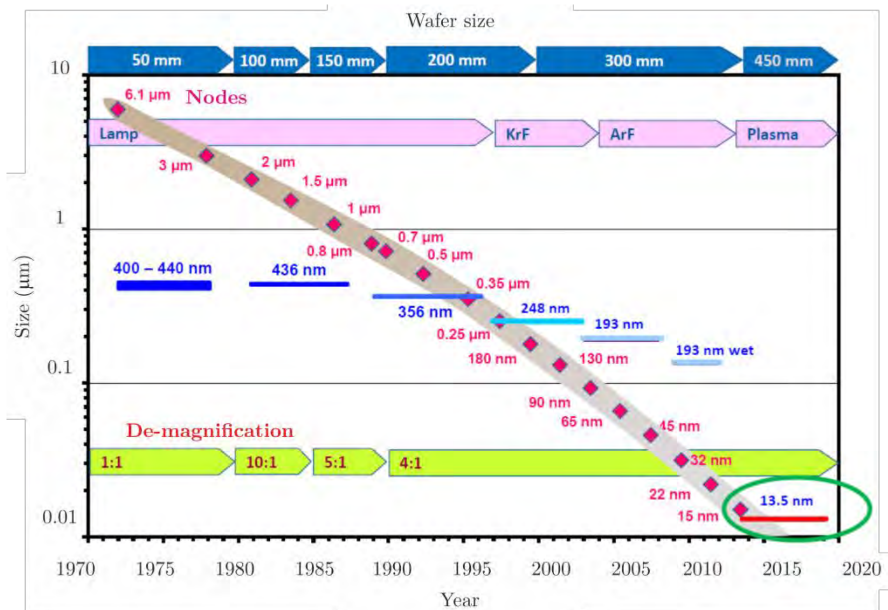

Figure 1.1. Lithography scaling map as a function of time and wafer size

In the next sections, the next generation lithography (NGL) techniques will be discussed, according to their challenges and their current status on the industry.

1.2.1. Optical lithography

Optical lithography has been the primary patterning method for semiconductor industry, since it has provided high-volume manufacturing and high-resolution chip production, as compared to other approaches.

As in other lithography approaches, the goal is to generate a pattern on a thin layer of resist, which is on the silicon substrate. Figure 1.2 shows a schematic representation of a general photolithography process.

The desired pattern is created on a photomask normally larger than the final pattern in the resist (4x in most systems), and the system has a projection lens which provides a demagnification ratio. Then, the resist is exposed to a pattern of intense light, which causes a chemical change on the exposed areas, which is finally developed. Thus, the final pattern on the resist is binary: there are parts covered with the resist, and others completely uncovered. Finally, this binary pattern is used for pattern transfer into the underlying layer.

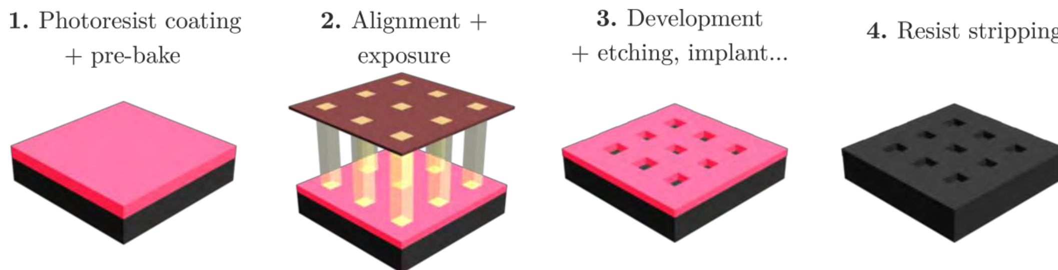

Figure 1.2. Schematic representation of a general photolithography process

The optical resolution *R*, is a key parameter in optical lithography, which depends on the illumination light wavelength, λ, and the NA of the projection lens, as shown in equation (1.1).

$$R = k \cdot \lambda / NA, \tag{1.1}$$

where k is a constant which depends on the resist and process technology NA is proportional to the medium index of refraction, n, and to the largest angle of converging rays subtended at the resist, θ. R can be reduced by reducing the wavelength and/or increasing NA.

When using optical lithography, changes in the NA, or in the material can improve the resolution, getting structures at fractional wavelength sizes.[4,5] The choice of the wavelength is determined by the radiation source. Figure 1.3 shows a schematic representation of the wavelength exposure systems. Until the late 1980s, optical lithography was performed with high-pressure Hg discharge lamps, which operated at 436 nm (g-line) and 365 nm (i-line), respectively.

Then, these lamps were substituted by more powerful excimer lasers, called deep-ultraviolet (DUV) systems, which have been the main pillar of the industry for the last past years. The excimer laser wavelengths for DUV are 248 nm (KrF) and 193 nm (ArF), respectively.[6] The 193 nm wavelength has allowed achieving resolutions of 50 nm. An important element of 193 nm lithography is the use of pellicles, which protect the mask from the contamination of particles, and maintains thus, the manufacturing yield of the industry. On the other hand, another related wavelength parameter is the resist, which cannot be too thin if it has to be used in pattern transfer. Therefore, large efforts on the development of new resists have to be performed, particularly in the chemically amplified resists (CAR).

As the resolution demands were increasing, the exposure wavelength was reduced to 157 nm by using F_2 lasers. Nevertheless, the development of lenses, masks, pellicles and resists took a considerable amount of time, and an alternative was found by introducing the ArF immersion system.[7] Immersion lithography replaces the air gap between the lens and wafer with a liquid which refractive index is greater than 1. By this way, the resolution is increased by a factor equal to the refractive liquid index.

The water immersion with ArF exposure allowed to overcome better the resolution limit of the ArF exposure, since it permitted getting wavelengths smaller than 157 nm, and resolutions of 39 nm.[8] 193 immersion lithography has displaced the 157nm technology, and has been the choice for printing critical dimensions of the 45 and 32 nm nodes.

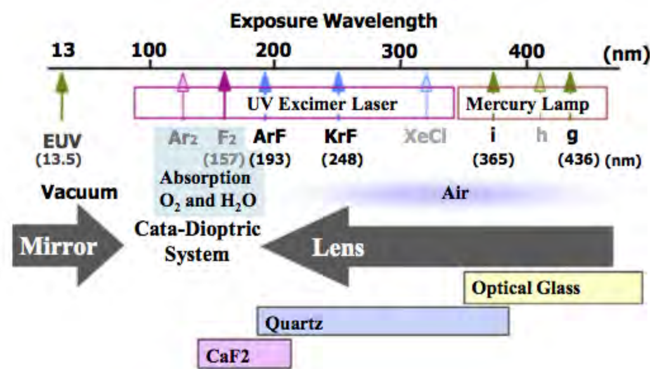

Figure 1.3. Wavelengths in projection exposure systems. Hg lamps are used for g-line and i-line exposure. In DUV, KrF and ArF excimer lasers are used[9]

1.2.2. Extreme ultraviolet lithography

EUV lithography development started in 1985, and it extends optical lithography to a higher resolution, since it utilizes a shorter wavelength (λ = 13.5 nm), as depicted in the scheme of Figure 1.3.

Moreover, EUV can greatly enhance the feature density of chips without using additional layers or multi-patterning, and it is currently developed for high volume manufacturing of the 7 nm logic node by 2020 (Intel, Globalfoundries, Samsung and TSMC).

The principle of EUV, is similar to optical lithography, in which the light is refracted through lenses onto the wafer. Nevertheless, because light radiation is strongly absorbed at this wavelength, all the EUV system must be in vacuum, and the optics must be reflective.

The EUV beam can be taken out from high-temperature and high-density plasma. There are mainly two methods two produce the plasma: the laser produced plasma (LPP) which produces plasma by condensing a strong laser beam into a material, and the discharge produced plasma (DPP) which produces plasma by a pulsed high-current discharge between electrodes in a certain atmosphere. The first one is the most commonly used in the industry, and its principle of operation is represented in Figure 1.4.

To generate the EUV light by the LPP system, the light source hits a rapid-fire stream of droplets with CO_2 laser pulses, which generates a plasma. The most common target material for laser-plasma are $_{50}Sn$, $_{53}I$, and $_{54}Xe$. The EUV excited from the plasma, is collected then by a condensing mirror, which directs the resulting radiation into the scanner, going through an intermediate focus which illuminates a reflection mask.

In summary, this means that, in order to generate EUV light of 13.5 nm wavelength, there is the need of a powerful laser, added to the disadvantage of having to work in vacuum and with specialized multilayer mirrors.

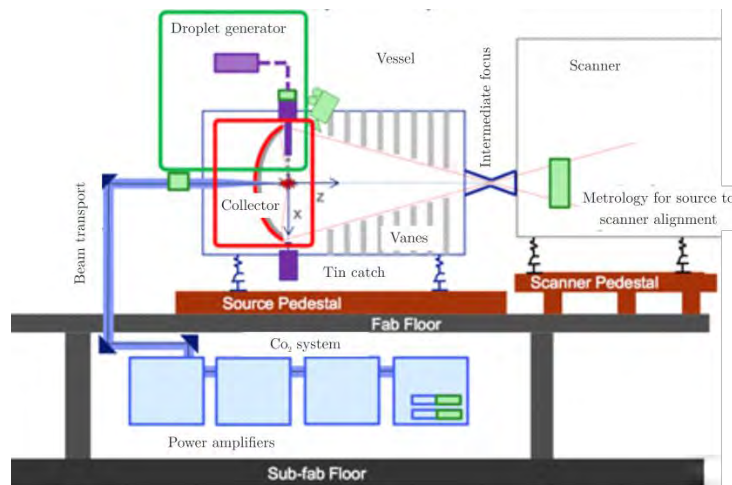

Figure 1.4. EUV generation principle (Image taken from *ASML*)

The major drawback of EUV, is that it does not only require new scan-systems, but also new chemicals and new mask infrastructure. Moreover, it has the big challenges of making masks free of defects, and on the other hand, of designing resists able to absorb EUV five times as faster.

All of these requirements make this technology to be very complex and expensive; more than twice that of an average 193 nm scanner. Although EUV presents these big challenges, there is being a very solid progress, and the industry is very optimistic about EUV lithography to be implemented into 7 nm logic node production.

Currently, manufacturers are using immersion lithography and multi-patterning at 16 nm, 14 nm and 10 nm logic nodes, respectively. However, for the 7 nm node, it seems that 193 immersion lithography is being replaced by EUV scanners due to its simplicity. Nevertheless, the 7 nm node will be costly not only for fabrication but for wafer, mask, design and development times costs.

1.2.3. Maskless lithography

Maskless lithography refers to the lithography approaches in which the radiation used to expose the resist is not projected or transmitted through a mask. The various forms of maskless lithography include: electron beam lithography (EBL), focused ion beam (FIB), interference lithography (IL) and scanning probe lithography (SPL).

1.2.3.1. Electron beam lithography

EBL is a complementary solution to optical lithography, because it offers a very high resolution (sub-10 nm) due to the achievable small wavelength (10-50 keV electrons). Nevertheless, it has a low throughput, and therefore its use is limited to mask fabrication, low-volume production and research and development.

Figure 1.5 shows a plot with the required time to expose an area of 1 cm^2, as a function of the minimum feature size. As observed in the graph, for linewidths below 600 nm, the exposure time does not meet with the minimum requirement of semiconductor industry (1 cm^2/s).

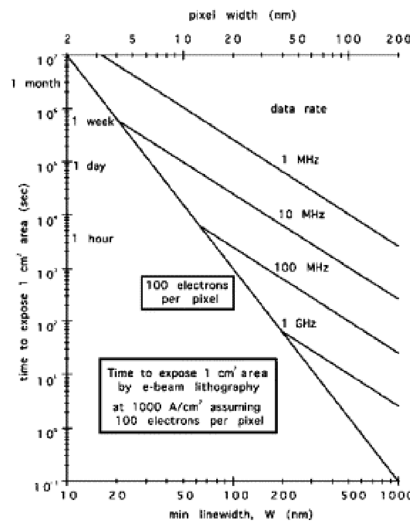

Figure 1.5. Required time to expose 1 cm^2 area with EBL as a function of the linewidth[10]

For research applications, normally an electron microscope equipped with an e-beam system is used, avoiding thus the extremely high costs of those used for commercial applications. These fully dedicated patterning systems present the advantage of offering very high resolution added to the ability of creating patterns without a mask. Moreover, despite presenting the drawback of using very long writing times, projection EBL[11,12] and the use of massive parallel beams[13] have been recently introduced to overcome these limitations.

The EBL fabrication principle involves the exposure of a highly focused electron beam to a resist in order to chemically modify its solubility and enabling the selective removal of either the exposed or non-exposed parts of the resist. The general fabrication process is depicted in Figure 1.6, which includes the (i) resist deposition, (ii) e-beam exposure, (iii) development and (iv) resist stripping. In between (iii) and (iv) other processes can be performed like etching or metallization.

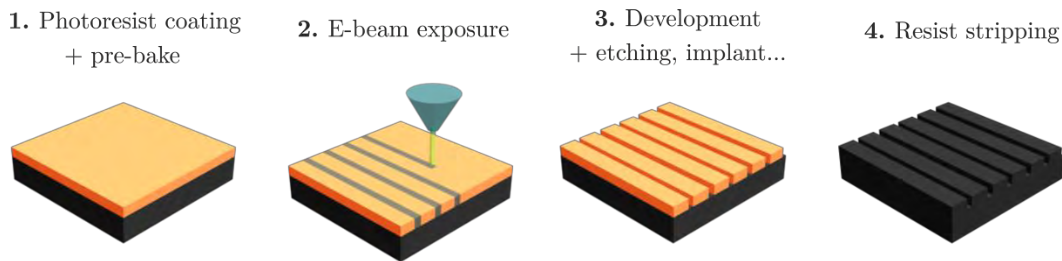

Figure 1.6. Schematic representation of a general e-beam process

The quality of the guiding patterns depends on the quality of the optics, resist, substrate and processing conditions (e-beam energy and dose, development time and temperature). On the other hand, the column containing the electron optics must operate in vacuum in order to reduce gas scattering of the beam.

The quality of the e-beam spot is determined by the electron optics and the degree of focus.[14] When the electrons go inside the resist, they start a sequence of collisions which produces the deflection of the beam. This effect, represented in Figure 1.7, increases with thickness and it is more pronounced at low energies.[15]

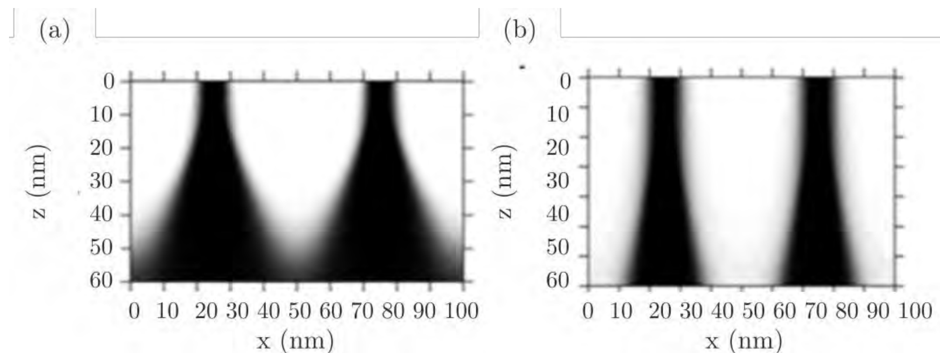

Figure 1.7. Simulations of electron beam broadening caused to scattering effects at (a) low and (b) high incident energies[16]

A part from the scattering effect, there is a need to control also the backscattering, produced by some electrons which eventually re-emerge into the resist (see Figure 1.8). This effect leads to beam broadening and proximity effects, causing pattern alterations and overexposure.[17,18]

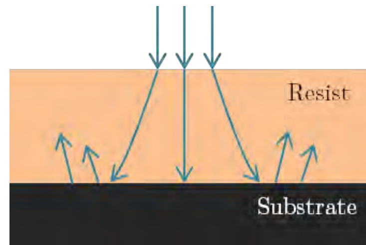

Figure 1.8. Backscattering of electrons and substrate

As shown in Figure 1.7 simulations, higher voltages produce high energy electrons which penetrate deeper and can spread laterally due to backscattering, increasing thus, the proximity effect. Although high voltages provide significantly high resolution and sharp resist profiles, low voltages (0.5 - 5 keV) are sometimes more convenient to reduce proximity effects, improve throughput and reduce the substrate damage caused to underlying materials.[19,20]

In summary, the EBL is a technique which although not used in high volume manufacturing, it is very suitable for research and development, and for masks production.

1.2.3.2. Focused ion beam

FIB instruments use an ion beam rather than electrons. The focused ion beam can directly mill the surface, with a nanometer controlled sputtering process. The ion source is normally Ga^{+}, since gallium has a low melting point, low volatility, low vapor pressure, and excellent mechanical, electrical and vacuum properties. Another ion source commercially available uses He ions, which are less damaging than Ga ions, but with low sputtering rates. Moreover, since He ions can be focused into small probe sizes, it offers higher resolution images.

FIB is normally assembled to a scanning electron microscopy (SEM) system, allowing thus, the generated features to be in situ visualized. In these systems, the electron and ion beams intersect at a 52° angle at a coincident point close to the sample surface.

The principle of operation is described in Figure 1.9. As observed in the scheme, applying an electrical field, the Ga ions are extracted from the metal surface by field transmission. These ions, are accelerated and focused through electrostatic lenses and then they hit the surface. Due to the interaction of the impinging ions with the surface, secondary electrons are generated and detected to produce an image. There are some ions which penetrate the sample and get trapped inside, producing their implantation. Ion implantation is commonly

used to introduce dopants into a semiconductor material. On the other hand, there are other ions, which transfer enough energy to the surface, inducing physical sputtering.

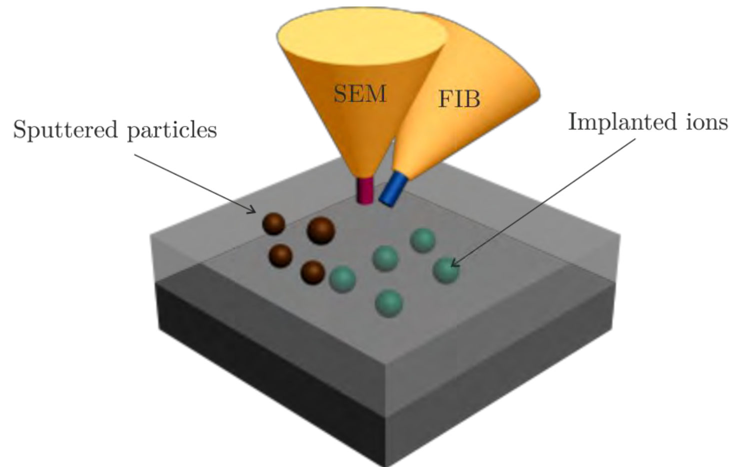

Figure 1.9. Schematic representation of a general FIB process

Figure 1.9 schematizes the different effects than can be produced simultaneously during the process: ion implantation, sputtering and secondary electrons due to the ion-matter collisions.

Another advantage of the FIB technique relies on the possibility of depositing material by directly adding a gas phase organometallic compound in the path of the ion beam. It decomposes when hits the ion beam and generates volatile organic compounds which are removed by the vacuum system, and metal remains which are deposited on the surface creating a thin film.

In summary, FIB offers numerous advantages to the semiconductor industry, like the ability to perform both milling and imaging, flexibility (different shapes and deposition of different materials), and fabrication of thin cuts around 100 nm thick. Moreover, its capabilities can be increased by building an in-situ electrical measurement, thus offering the possibility of performing electrical measurements while the FIB is operating.

1.2.3.3. Interference lithography

IL is a technique which uses two interfering light beams to produce periodic structures. Its basic principle is the same as interferometry introduced by *Thomas Young* in 1801, in which the light is divided and recombined, formic periodic intensity patterns that are recorded into the substrate (see Figure 1.10). Then, the resist is exposed to the two superimposed single laser beams.

For two interfering beams, the periodicity of the patterns is given by:

$$P = \lambda / (2 \cdot \sin \theta), \quad (1.2)$$

where λ is the wavelength, and θ is the angle between the two interfering waves.

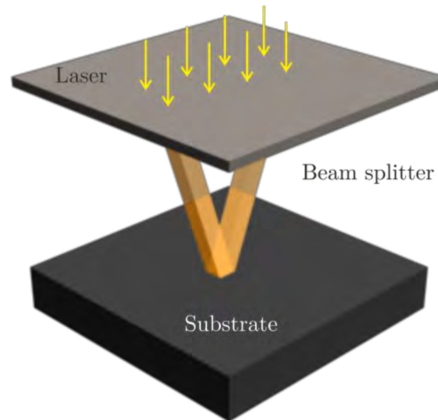

Figure 1.10. Interference of two coherent laser beams

The most interesting advantage is that dense features over a wide area can be produced without losing the focus. Therefore, it is commonly used for the fabrication of molds in NIL[21], or for testing resist processes for lithography approaches with new wavelengths. Nevertheless, its use its limited to patterning features uniformly distributed, and other types of lithography have to be used if arbitrarily shaped patterns are desired.

1.2.3.4. Scanning probe lithography

SPL emerged in the late 1980s. It is based in scanning tunneling microscopy (STM) or atomic force microscopy (AFM), and they are used to pattern features in the nanometer range. Its mechanism is based on using a sharp tip in proximity to the sample to pattern the desired features.

Figure 1.11 shows the general SPL generation system. As observed, a local tip is brought close to the surface (nanometric distance), and the resulting tip-sample interactions (electrical, optical or mechanical) are measured in real time.

The position of the tip is controlled in the three directions by means of piezoelectric tubes. In AFM, the interaction signal is the deflection of a laser beam focused on a cantilever on which the tip is attached, whereas in STM, the interaction signal is the measurement of the tunnel current between the top and the surface of the conducting surface.

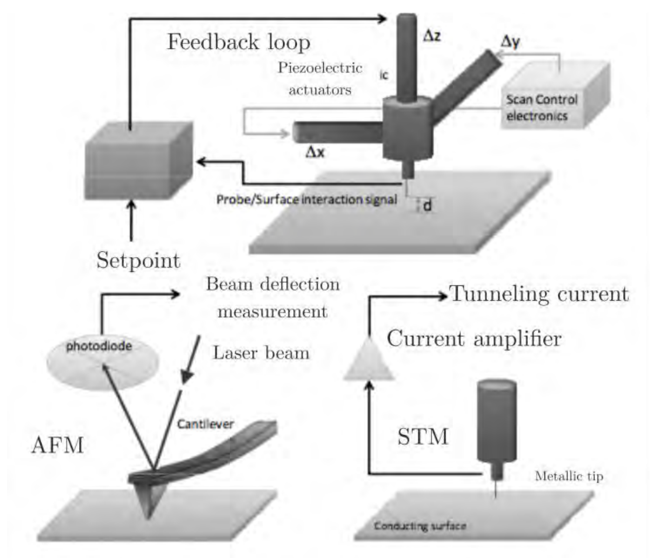

Figure 1.11. Schematic representation of a general SPL process

Apart from providing information about the surface local properties, SPL can be also used to modify the surface in a permanent way. These processes can be thermal, electrical, mechanical or diffusive.[22] Figure 1.12, shows the classification of the SPL methods depending on the tip-surface interaction.

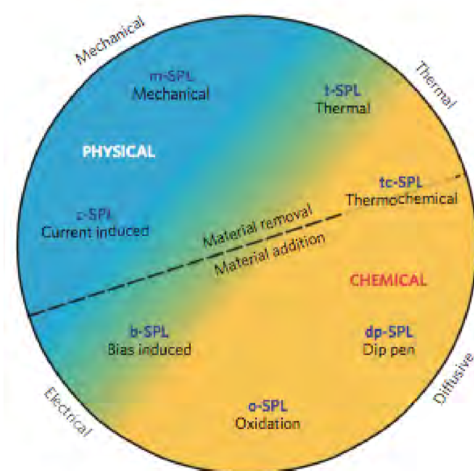

Figure 1.12. Classification of the SPL methods depending on the tip-surface interactions[22]

SPL techniques offer a wide range of approaches to modify the surface, and thus leads to a high variety of patterning methods. On the other hand, as compared with other techniques, it presents the advantage of pattering in ambient conditions with no special material requirements and with high resolution.

Nevertheless, it has very low throughput is unsuitable out of the laboratory environment. To overcome these issues, different approaches are being studied, like the use of multiple probes, which can read and write in parallel.[23]

1.2.4. Nanoimprint lithography

NIL is a low cost process, which offers high throughput and resolution. Its basic principle has been known for hundreds of years. However, its sub-100 nm application was introduced by *Stephen Chou* in 1995.[24]

The fabrication process of NIL is depicted in Figure 1.13, and it consists in imprinting nanostructures from a mold to a surface, pressed into a thin resist deposited on the substrate. There are different NIL techniques, but the mostly used are the thermal NIL (Figure 1.13.a) and the UV NIL (Figure 1.13.b), respectively.

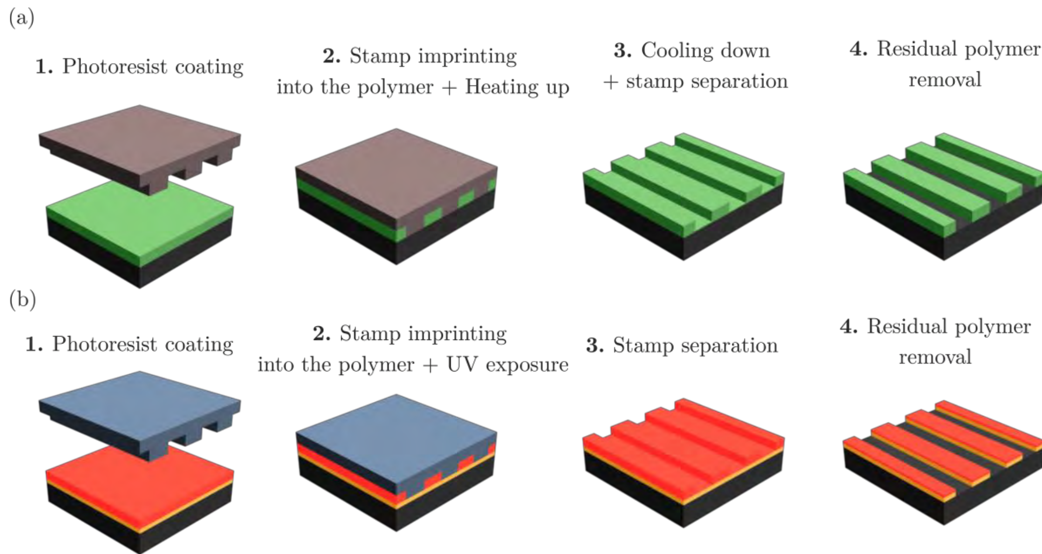

Figure 1.13. Schematic representation of a general (a) thermal and (b) UV nanoimprint process

The thermal NIL is the conventional process developed by *Stephen Chou.* During the imprint process, the mold is kept in contact with the resist, and they are heated up above the glass transition temperature of the polymer in order to make it softener.[24] Hereafter, the polymer is cooled down and the mold is removed, leaving the pattern resist left on the substrate.

On the other hand, in UV NIL, transparent molds are imprinted into UV curable liquid resists at room temperature. Then, the mold and the substrate are put in contact and pressed. During this process, the resist is cured in UV light and becomes solid. Subsequently, the mold is removed.

Unlike conventional lithography methods, NIL does not require the use of energetic beams. Therefore, the mold used can be made by a high-resolution and low-throughput lithography, and the NIL can be used for low-cost high-volume manufacturing. Furthermore, it is a versatile technique with applications that go beyond microelectronics, including optics, plasmonics or biotechnology.

Despite the amount of benefits, there are still important challenges to overcome: throughput, overlay and defect density. For quite a long time, the throughput has improved, coming from faster filling times of the resist into the mold (80 wafers per hour). On the other hand, the overlay (ability of the lithography scanner to align and print the various layers accurately on top of each other) is also improving by the development of new wafer chucks to improve the flatness around the wafer meeting the production standards by 2018. Regarding the defectivity, it is expected to improve, as the technology develops, by improving the template cleaning, resist materials and by employing antistiction layers on the stamp to reduce the adhesion between it and the resist.

1.2.5. Directed self-assembly of block copolymers

Lithography using BCPs was first introduced by *Mansky et al.*, in 1995.[25] The most interesting feature of a BCP is the ability to self-assemble into domains with dimensions that are very expensive to fabricate with conventional lithographic tools. The first study with BCPs, was with a poly(styrene-*b*-butadiene) (PS-*b*-PB) system, in which the BCP film was annealed to form a single layer of PB spheres into a PS matrix.[25]

DSA has become a relevant alternative lithographic technique for the creation of nanometer scale patterns due to its high throughput and process simplification compared to other approaches.[26,27] It is important to remark that DSA is not a stand-alone lithography, but a combination of a lithographic tool with the ability of BCPs to self-assemble into nanoscale features. Moreover, DSA is a potentially viable patterning technique for the semiconductor industry since it offers higher throughput and simpler and lower cost processes compared to other techniques.[28]

Even though, the major drawbacks of DSA are related with placement and defectivity. However, significant progress has been achieved in the past few years up to the extent that defect levels have been dramatically reduced (defectivity values around 24 defects/cm^2).[29,30] The industry is struggling nowadays with DSA design and integration challenges.[31]

There are two main approaches to control the orientation and alignment of self-assembled BCP domains: *graphoepitaxy*[32,33] and *chemical epitaxy*.[34–36] Figure 1.14 shows a schematic representation of a general DSA process by graphoepitaxy (Figure 1.14.a) and by chemical epitaxy (Figure 1.14.b).

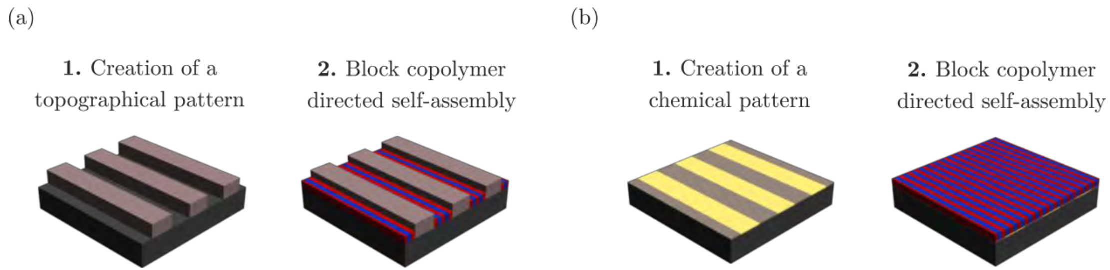

Figure 1.14. Schematic representation of a general DSA process by (a) graphoepitaxy and (b) by chemical epitaxy

On the one hand, graphoepitaxy is based on using topographic patterns (usually holes or trenches) and confine the BCP on it. It is commonly used in combination with cylindrical BCPs in order to shrink the size of contact holes or to achieve contact-hole multiplication.

On the other hand, chemical epitaxy consists of creating chemical patterns on a neutral surface so that the modified areas would present larger affinity to one of the blocks, determining the position and orientation of the molecules. The major difference between topographical and chemical DSA is the relative length scale between the pattern and the pitch of the BCP.

Until now, the multiplication factors in graphoepitaxy can be four times larger than the BCP pitch, which are much larger than in chemoepitaxy. One of the major advantages of chemical epitaxy with respect to graphoepitaxy is the reduction of the edge roughness due to the self-healing of BCPs, which means that the irregularities of the guiding patterns are not certainly transferred to the BCP pattern.[37]

Some years ago, the original projections were all for DSA, and it was supposed to move into the logic production flow from the 14 nm to 7 nm node. However, together with its principal problem, the defectivity, pattern roughness, placement accuracy and material quality control, are still challenges that need to be overcome.

Currently, DSA of PS-*b*-PMMA defined on chemical guiding patterns is the primary focus of activities, and therefore, the main research objectives involve demonstrations that DSA can meet manufacturing requirements in terms of defectivity. On the other hand, the industry is also working on other DSA materials which scale beyond 11 nm, the minimum size achievable for PS-*b*-PMMA.

For the near future, DSA is not ready for insertion into industry for conventional patterning, but it will be used for pattern healing or repair. Nevertheless, by reducing the defectivity and improving patterning reliability, DSA patterning can push 193 nm lithography beyond its limits, especially for space/line applications by using chemical epitaxy.

1.3. Summary: lithography status, issues and challenges

Lithography is a key technology for semiconductor industry since it determines the device critical dimensions. The permanent quest for miniaturization is becoming increasingly difficult, since the cost and functionality of the fabrication processes are increasing and becoming more complex.

The recent ITRS lithography roadmap shows a big technology decision about how to lead the next generation logic node. As shown in Figure 1.15, multiple patterning and all the NGL techniques have enough resolution to reach the 10-nm half-pitch and better.

Although EUV seemed to be the preferred option for the next generation nodes, some required improvements are taking longer than expected, and NIL and DSA are becoming much closer to manufacturing implementation. Especially DSA has demonstrated improved defectivity and progress in process flow integration.

Experts on the field, support the idea that EUV is the most suitable technique for the next generation node, but probably only has one more generation before having to add multi-patterning or much larger NA.

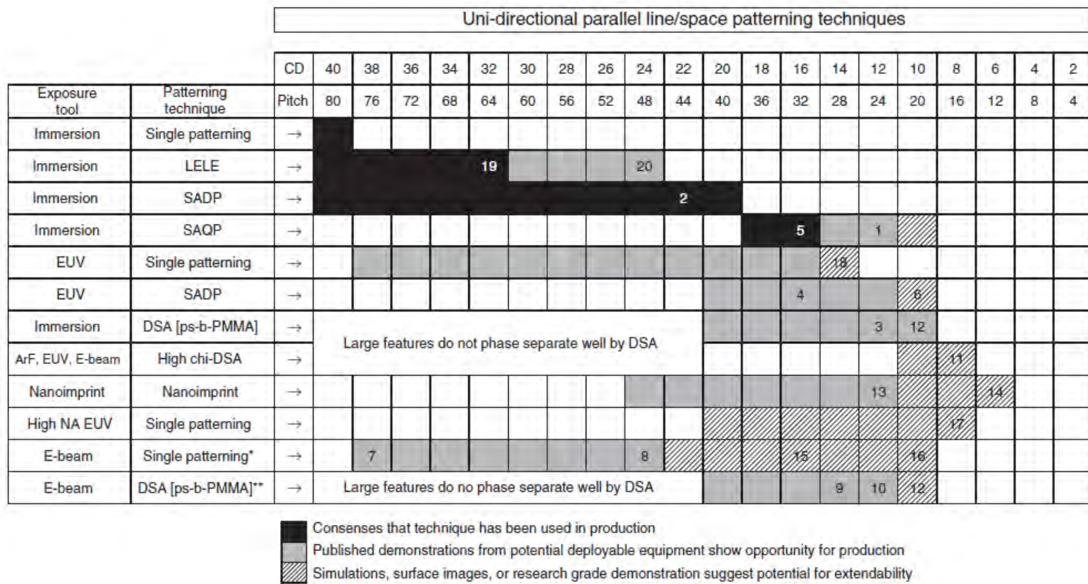

Figure 1.15. Potential solutions for line/space applications by pitch and half pitch published in the 2013 ITRS Roadmap for Lithography

To summarize, DSA and NIL are very promising techniques at lower cost, EUV promises a simpler and shorter processes, and mask-less lithography is becoming more focused for chip personalization and cost effective for low volume chip designs.[38] Nevertheless, EUV is still not ready for high-volume manufacturing at 7 nm node, which is predicted for 2018 to 2019. Although it is making a noticeable progress, there are still some challenges ahead, such as power source, resists and pellicles.

In any case, it seems that bringing technology from the laboratory to the fabrication is becoming more difficult at each node, probably because technology has been pushed much further than it was predicted to be.

1.4. References

1. Moore, G. E. Cramming more components onto integrated circuits. **38,** (1965).

2. Moore, G. E. Progress in Digital Integrated Circuits. *IEDM Tech. Dig.* (1975).

3. Jackson, T. N. Beyond Moore ' s Law. *Nat. Mater.* **4,** 581–583 (2005).

4. Ito, T. *et al.* Pushing the limits of lithography. *Nature* **406,** 1027–1031 (2000).

5. Yoo, P. J., *Suh, K. Y., Kim, Y. S., Brugger, J. & Legget, G. J.* (2005).

6. Rothschild, M. *et al.* Excimer projection lithography at 193 nm wavelength. *Proc. SPIE* **922,** (1988).

7. Bloomstein, T. M. *et al.* Lithography with 157 nm Lasers. *J. Vac, Sci. Technol. B* **15,** (1997).

8. Lin, B. J. Semiconductor foundry, lithography, and partners. *Proc. SPIE* **4688,** (2002).

9. Okazaki, S. High resolution optical lithography or high throughput electron beam lithography: The technical struggle from the micro to the nano-fabrication evolution. *Microelectron. Eng.* **133,** 23–35 (2015).

10. Menon, R., *et al.* Maskless lithography. *Mater. Today* **8,** 26–33 (2005).

11. Liddle, J. A. *et al.*High-throughput projection electron-beam lithography employing SCALPEL. *Proc. SPIE* **2014,** 66–76 (1993).

12. Pfeiffer, H. C. *et al.* PREVAIL – IBM's e-beam technology for next generation lithography. *Futur. Fab Int.* **12,** (2002).

13. Hakkennes, E. A. *et al.* Demonstration of real-time pattern correction for high-throughput maskless lithography. in **7970,** 79701A–79701A–11 (2011).

14. Goldstein, J. *et al. Scanning Electron Microscopy and X-ray Microanalysis.* (Spinger US, 2003).

15. Lee, Y. -H., *et al.* Low voltage alternative for electron beam lithography. *J. Vac. Sci. Technol. B Microelectron. Nanom. Struct. Process. Meas. Phenom.* **10,** 3094–3098 (1992).

16. Stepanova, M. *et al. Nanofabrication: Techniques and principles. Nanofabrication: Techniques and Principles* (2014).

17. Chang, T. H. P. Proximity effect in electron-beam lithography. *J. Vac. Sci. Technol.* **12,** 1271–1275 (1975).

18. Lo, C. W., *et al.* Resists and processes for 1 kV electron beam microcolumn lithography. *J. Vac. Sci. Technol. B Microelectron. Nanom. Struct. Process. Meas. Phenom.* **13,** 812–820 (1995).

19. Yau, Y. W., *et al.* Generation and applications of finely focused beams of low-energy electrons. *J. Vac. Sci. Technol.* **19,** 1048–1052 (1981).

20. Sugita, A. *et al.*Resist Exposure Characteristics by a Focused Low Energy Electron Beam. *J. Electrochem. Soc Solid-State Sci. Technol.* **135,** 1741–1746 (1988).

21. Bläsi, B. *et al.* Large area patterning using interference and nanoimprint lithography. *Proc. SPIE* **9888,** (2016).

22. Garcia, R., *et al.* Advanced Scanning Probe Lithography. *Nat. Nanotechnol.* **9,** 577. (2014).

23. Vettiger, P. *et al.* the 'Millipede'-Nanotechnology Entering Data Storage. *Trans. Nanotechnol.* **1,** 39–55 (2002).

24. Chou, S. Y., *et al.* Imprint Lithography with 25-Nanometer Resolution. *Science.* **272,** 85–87 (1996).

25. Mansky, P., *et al.* Monolayer films of diblock copolymer microdomains for nanolithographic applications. *J. Mater. Sci.* **30,** 1987–1992 (1995).

26. Liu, G., T *et al.* Integration of Density Multiplication in the Formation of Device-Oriented Structures by Directed Assembly of Block Copolymer-Homopolymer Blends. *Adv. Funct. Mater.* **20,** 1251–1257 (2010).

27. Rathsack, B. *et al.* Advances in directed self assembly integration and manufacturability at 300 mm. **8682,** 86820K (2013).

28. Hinsberg, W., *et al.* Self-Assembling Materials for Lithographic Patterning: Overview, Status and Moving Forward. *Proc. SPIE* **7637,** (2010).

29. Rincon Delgadillo, P. *et al.* Defect source analysis of directed self-assembly process (DSA of DSA). *Proc. SPIE* **8680,** 86800L–86800L–9 (2013).

30. Gronheid, R. *et al.* Defect reduction and defect stability in IMEC's 14nm half-pitch chemo-epitaxy DSA flow. **9049,** 904905 (2014).

31. Somervell, M. *et al.* Driving DSA into Volume Manufacturing. **9425,** 1–11

32. Park, S. *et al.* Macroscopic 10-terabit-per-square-inch arrays from block copolymers with lateral order. *Science* **323,** 1030–1033 (2009).

33. Tiron, R. *et al.* Pattern density multiplication by direct self assembly of block copolymers: toward 300mm CMOS requirements. *Proc. SPIE* **8323,** 83230O–83230O–7 (2012).

34. Tada, Y. *et al.* Directed Self-Assembly of Diblock Copolymer Thin Films on Chemically-Patterned Substrates for Defect-Free Nano-Patterning. *Macromolecules* **41,** 9267–9276 (2008).

35. Kim, S. O. *et al.* Epitaxial self-assembly of block copolymers on lithographically defined nanopatterned substrates. 411–414 (2003).

36. Edwards, *et al.* Long-Range Order and Orientation of Cylinder-Forming Block Copolymers on Chemically Nanopatterned Striped Surfaces. 3598–3607 (2006).

37. Stoykovich, M. P. *et al.* Directed Assembly of Block Copolymer Blends into Nonregular Device-Oriented Structures. **1442,** (2014).

38. Neisser, M. *et al.* ITRS lithography roadmap: 2015 challenges. *Adv. Opt. Technol.* **4,** 235–240 (2015).

Chapter 2

Chemistry and physics of block copolymer materials

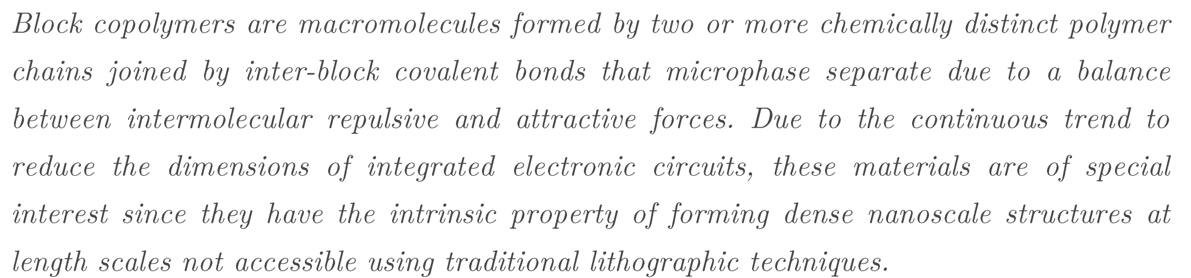

Block copolymers are macromolecules formed by two or more chemically distinct polymer chains joined by inter-block covalent bonds that microphase separate due to a balance between intermolecular repulsive and attractive forces. Due to the continuous trend to reduce the dimensions of integrated electronic circuits, these materials are of special interest since they have the intrinsic property of forming dense nanoscale structures at length scales not accessible using traditional lithographic techniques.
This chapter aims to give the fundamentals of block copolymers, including their synthesis and self-assembly properties.

2.1. Block copolymers and their synthesis

A copolymer is the result of a polymerization between two or more different monomers, and they are classified based on how these monomers are arranged in the chain[1], as shown in Figure 2.1. More complex architectures also exist, where different chains can form each branch.

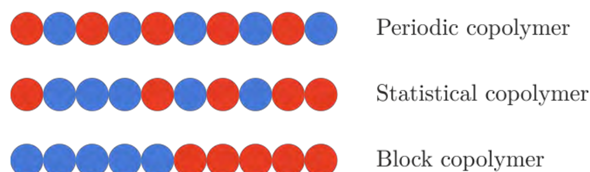

Figure 2.1. Representation of the different copolymer types

BCPs are macromolecules formed by two or more chemically distinct repeat units joined together by covalent bonds.[2] These materials have attracted special interest in the last few years because of their ability to self-assemble into ordered structures at the nanometer scale.[3–6] The most characteristic feature of a BCP is the strong repulsion that exists between the different domains. As a result of this repulsion, BCPs tend to segregate, but as they are chemically bonded, even with a complete segregation, they cannot lead to a macroscopic phase separation, as in the case of a polymer blend. Rather, different polymers chains minimize their repulsive energy by segregating into microdomains with a length scale on the order of tens of nanometers or less. At low temperature the enthalpic effect drives the blocks to phase-separate, while at high temperatures entropic effects dominates and results in an homogenous mixture, as depicted in Figure 2.2.

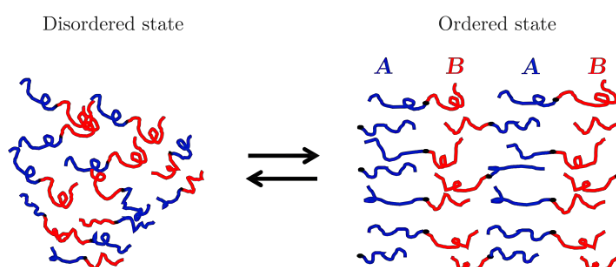

Figure 2.2. Schematic representation of disordered and ordered states of an A-B diblock copolymer

In order to synthesize a well-defined BCP, a controlled chain-growth polymerization method is needed together with an appropriate purification method. There are numerous routes to synthetize BCPs, but radical polymerization is one of the most used for commercial production of high molecular weight polymers, since it is more competitive by providing simple and reproducible mechanisms.[7] Methods involving radical processes have been the most relevant and widely used since they can be used by a large variety of monomers and they allow very broad range of processing conditions. Nevertheless, the

conventional processes present some drawbacks regarding the molecular weight distribution, composition and the fact that some residual monomer remains even after long reaction times.

In the radical polymerization processes, as depicted in Figure 2.3, the first step consists on the production of free radicals by thermal or photochemical decomposition of specific compounds, or by using high energy radiation and reduction-oxidation reactions. These free radicals react with a monomer in a way that the new molecule becomes the new free radical. Therefore, the growth of a polymer chain consists in the successive addition of monomers during propagation. The propagation step continues until all monomers are consumed. Then, the polymerization process is finished either by combination in which two growing polymer chains react with each other, or by disproportionation in which an hydrogen atom is transferred from one radical to the other resulting in two polymers. In this conventional polymerization method, the molecular weight increases rapidly at early stages and then is reduced because of monomer exhaustion. However, in an ideal polymerization process all the chains have to grow at the same time and survive the polymerization. This can only be possible in the presence of reagents that react with radicals (RM ·) by reversible deactivation or reversible chain transfer, as described in Figure 2.4. In that case, the lifetime of an individual chain as an active specie will be lower.

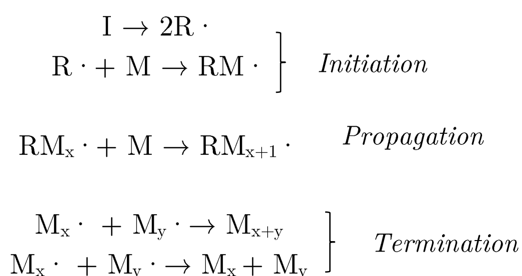

Figure 2.3. Schematic representation of conventional radical polymerization process (I, R · and M denote the initiator, radical and monomer species, respectively)

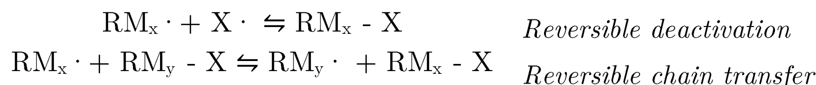

Figure 2.4. Schematic representation of radical polymerization process with reversible deactivation and chain transfer

Different living polymerization techniques have been used for the synthesis of BCPs, like nitroxide-mediated polymerization (NMP)[8], atom-transfer polymerization (ATRP)[9,10] or reversible addition-fragmentation chain transfer (RAFT)[11,12], being this last one the most convenient and useful[13,14] since it is applicable under a large number of experimental conditions. RAFT process involves conventional radical polymerization in the presence of a suitable chain transfer agent (thiocarbonylthio RAFT agent) which mediates the polymerization process by a reversible chain-transfer process, allowing the production of low polydispersity (PDI) and high-functionality polymers. Normally, the suitable RAFT agent

described in Figure 2.5 has a thiocarbonylthio group with substituents R and Z that influence the polymerization reaction kinetics.

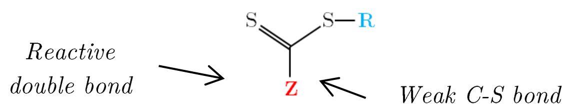

Figure 2.5. General structure of RAFT agent. R and Z are group substituents of the molecule

Figure 2.6 shows a schematic representation of how the RAFT polymerization mechanism takes place. During the initiation process (shown in the first step of Figure 2.3) the initiator is decomposed into fragments (R ·) which react with a single monomer molecule, growing a polymeric radical (RM_x ·). Polymeric radicals react in the next step with the RAFT agent to create an intermediate RAFT product which can lose either the R group (R ·) or the polymeric species (RM_x ·). After, the leaving group reacts with another monomer to create a new propagating radical referred as RM_y. Then, there is a rapid equilibrium between the active radicals and all the species that have not undertaken termination. This is the most important step in the RAFT process, and it provides equal probability to all chains to grow with narrow PDI. Finally, when the polymerization is completed, active chains react to form chains that cannot react further.[15] For BCPs, there is the additional limitation that the RAFT agent must be suitable for both monomers.[16]

The RAFT process has emerged as one of the most important methods of living polymerization for BCP synthesis, since it can provide control over the way of initiation and termination steps and have a better chain length polymer control, a part of presenting versatility in the use of a wide number of monomers and processing conditions.

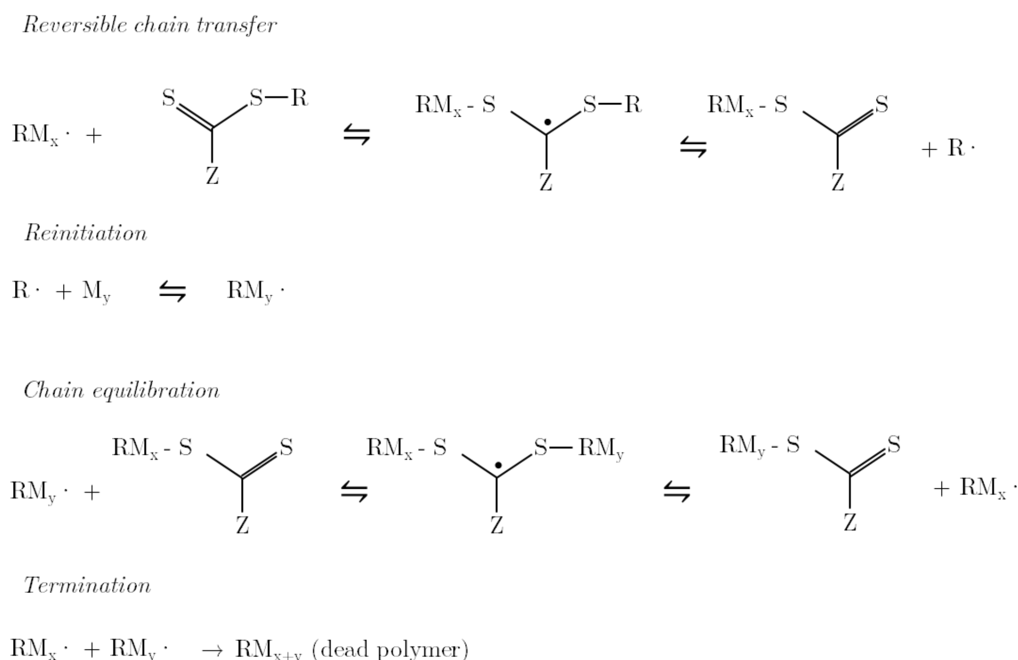

Figure 2.6. Schematic representation RAFT mechanism process

2.2. Physics of block copolymers

2.2.1. Order-disorder transition in block copolymers

The change in free energy of mixing (ΔF_m) when applied to polymer blends is described by the *Flory-Huggins* theory[17] in which it is assumed that components are incompressible and mix at constant volume.[18] Equation (2.1) represents the dependence of ΔF_m with the entropy contribution (ΔS_m, first two terms) and the enthalpy input (ΔH_m, third term) which includes the *Flory-Huggins* parameter, χ.

$$\frac{\Delta F_m}{k_B T} = \frac{\emptyset_A}{N_A} \ln \emptyset_A + \frac{\emptyset_B}{N_B} \ln \emptyset_B + \chi \emptyset_A \emptyset_B , \tag{2.1}$$

where ϕ_A and ϕ_B are the volume fractions of species A and B in the blend, N_A and N_B are the degree of polymerization of species A and B, $k_B T$ is the thermal energy, and χ is the *Flory-Huggins* parameter.

In contrast with homopolymer blends, diblock copolymers cannot separate macroscopically, but form ordered microphase separated morphologies due to the fact that the blocks are joined by covalent bonds and this leads to the formation of different phases depending on the volume fraction of each domain. Therefore, the *Flory-Huggins* theory is unsuitable to study the microphase separation of a BCP. *Bates and Fredrickson* have reviewed the extensive experimental and theoretical thermodynamics of BCPs.[3]

The phase behavior of an A-B BCP is determined by three main parameters: (i) the overall degree of polymerization, N, (ii) the volume fraction of each domain in the BCP, f, and (iii) the *Flory-Huggins* interaction parameter, χ, which represents the energy cost of two species to be mixed homogeneously and is inversely proportional to temperature. The first two parameters are dictated by the polymerization stoichiometry and the translational and configurational entropy, whereas χ is determined by the selection of the material, which has a largely enthalpic contribution. Thus, the strength of the BCP segregation power is normally expressed by the reduced parameter χN, which reflects both enthalpic and entropic contributions. By increasing χ, which favors a reduction in A-B contacts, and N, which is related to some loss of translational and configurational entropy, a local compositional ordering frequently referred to as *microphase separation* is induced. On the contrary, if either N or χ are not large enough, the entropic contributions will dominate leading to a disordered phase.

The critical point predicted by mean-field calculations for symmetric diblock copolymers is $\chi N = 10.5$.[19] There exists two regimes in BCPs microphase segregation: strong[20,21] and weak[19,22] segregation. In the strong segregation limit (SSL), where $\chi N \gg 10.5$, the interaction energy drives the blocks to segregate into well-defined microdomains and the A-B interface is narrow. In the weak segregation limit (WSL), which occurs in the vicinity of the order-disorder transition, the entropic terms are larger than the interaction term.

Therefore, the two blocks are miscible since the segregation power is not strong enough to form a sharp phase boundary between the two phases, thus the interface becomes diffuse. The boundary between the melted and segregated structures is determined by the order-disorder temperature, T_{ODT}, where the thermal energy is comparable to the interaction energy of the two blocks. For $f = 0.5$, the transition between ordered and disordered states occurs when χN is approximately 10.[23] When $\chi N \ll 10.5$, entropy dominates the energetic penalty of mixing A and B segments, resulting in a disordered phase. As this value increases, A and B domains remain ordered in the microscopic scale since they are chemically joined.

2.2.2. Morphologies of diblock copolymers

As previously described, the structure resulting from the BCP microphase separation will depend on the degree of polymerization, the composition of the BCP and the chemical interaction between blocks. The phase behavior of an A-B diblock copolymer has been studied experimentally[24] and a successful theoretical correlation has been found by using the self-consistent field theory (SCFT).[21,25–27] Based on SCFT, *Matsen and Bates*[27] constructed a phase diagram for an A-B copolymer from the WSL to the SSL, and it was observed that for the WSL the SCFT results agree with *Leibler* who first showed the phase diagram in this region.[19]

Figure 2.7 shows the most updated phase-diagram for an A-B diblock copolymer[28] which consists on a representation of χN as a function of *f*. The BCP morphology will depend basically on the strength of the interactions between monomers and the bulk fraction of each domain. The phase diagram shows that by increasing *f*, body-centered cubic (bcc) spherical (S), hexagonal-close packed (hcp) spherical (S_{cp}), cylindrical (C), gyroid (G) and lamellar (L) structures are predictable. Figure 2.8 shows a schematic of the most useful microphase arrangements of blocks in an A-B diblock copolymer as a function of *f*.

Over the years, there have been several contributions to the phase diagram, and lately another morphology was identified both theoretically[29] and experimentally corresponding to the *orthorombic Fddd* phase (O^{70}).[30–33] On the other hand, it can be inferred that for a symmetric system, below $\chi N = 10.5$ the system is disordered, and between 10.5 and 12.5 it is found the WSL, in which it is expected to appear some disordered regions due to thermal effects derived from the fact that the thermodynamic driving force, is small.

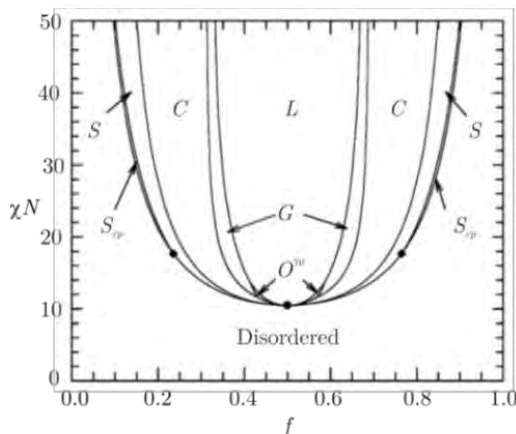

Figure 2.7. Phase diagram for an A-B diblock copolymer showing the ordered lamellar (L), cylindrical (C), spherical (S), gyroid (G) and *Fddd* (O^{70}) morphologies[28]

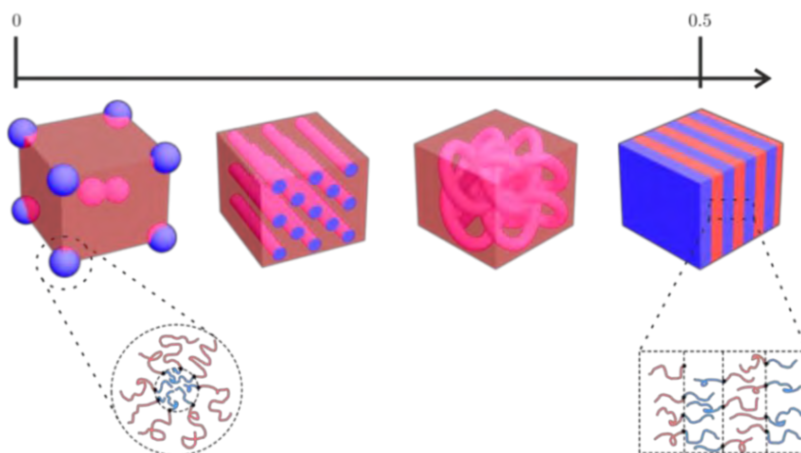

Figure 2.8. Schematics of the most common ordered-state morphologies found in an A-B diblock copolymer as a function of *f*. Above f = 0.5, the hierarchy reverses, i.e. the morphology phases repeat with the blocks reversed

For non-crystallizable homopolymers there is a thermal transition where upon heating, the material changes from a vitreous solid to the viscous or rubbery liquid state. This temperature is called *glass transition temperature,* T_g, and above it polymer chains have greater mobility since polymer free volume increases. BCPs exhibit two T_g corresponding to its constituent blocks, so in order to allow BCP molecules diffuse freely, it has to be heated above the largest T_g, and the film becomes more ordered over time. Nevertheless, there is a limit on temperature which is set by the stability of the polymer that can undergo crosslinking or chain scission.

2.2.3. Block copolymers in thin films

In lithographic applications, BCPs are used to form thin films, so the phase behavior is actually richer than in bulk, since there are effects induced by the interfaces involving air and the substrate. Generally, thin films are produced by coating a substrate with a dilute polymer solution in an appropriate solvent for both blocks. BCPs show the same

morphology as in bulk, but the orientation of the phase strongly depends on the boundaries, i.e. on the interaction between the domains and the substrate.

2.2.3.1. Role of surface affinity

Figure 2.9 shows a cylindrical A-B diblock copolymer self-assembled onto two different systems. When the substrate has a neutral attraction for both domains, the cylinders are oriented perpendicular to the substrate, whereas if the substrate strongly attracts one of the domains, the free energy is minimized by forming a layer with cylinders oriented parallel to the substrate.

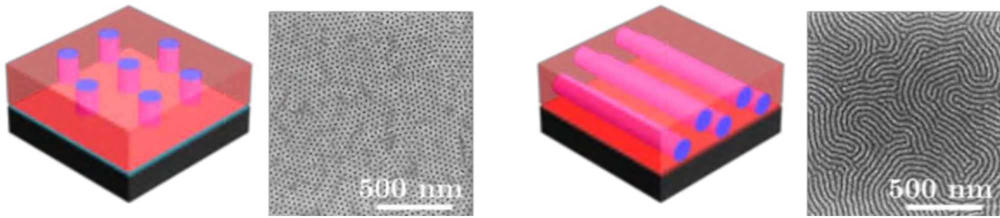

Figure 2.9. Schematic and SEM images of cylindrical PS-b-PMMA block copolymer, showing different polymer blocks-surface interactions

2.2.3.2. Role of block copolymer film thickness

In a thin film, the BCP morphology is strongly influenced by the boundary conditions determined by the surface and the interface of the film. The total free energy of an A-B diblock copolymer thin film can be expressed as a sum of the contributions from its internal structure, F_{bulk}, and from its surface/interface, F_{surf}, as shown in Equation (2.2):

$$F = F_{bulk} + F_{surf} = \left(F_{A/B} + F_{conf}\right) + \left(F_{A/subs} + F_{B/subs} + F_{A/air} + F_{B/air}\right), \quad (2.2)$$

where $F_{A/B}$ is the interfacial energy between A and B, F_{conf} is the conformational entropy of A and B, and $F_{A/air}$, $F_{B/air}$, $F_{A/subs}$ and $F_{B/subs}$ are the interaction energies between each domain and the air or substrate, respectively.

Normally, in a directed self-assembly (DSA) process, BCP film thickness, *d*, is less than few nanometers the BCP pitch, L_0, and therefore the contribution of the surface to the total free energy, *F*, becomes a significant. Therefore, the effect of commensurability between BCP film thickness, *d,* and its natural period, L_0, is vitally important, and it makes the film thickness to be an integer or half-integer of L_0. If not, the energy due to the conformational entropy of the A and B polymer chains becomes too high and leads to non-homogeneous BCP films.

Figure 2.10 shows a general overview of the different morphologies a lamellar diblock copolymer can present depending on the interface energies between the domains and the air and substrate, respectively. As it can be observed, the surface and air are in contact with the polymer which presents lower interface energy and the BCP is oriented parallel to the

substrate when domains present different interface energies with air and substrate. In that situation, one has to take into account that the film thickness has to be equal to n · L_0 or (n+0.5) · L_0, in order to not change the natural bulk period, L_0. When film thickness does not commensurate with n · L_0 or (n+0.5) · L_0, the system tends to minimize its free energy by forming spontaneously macroscopic islands or holes. On the other hand, perpendicular lamellae are observed when both the air and the substrate present equal affinity for both BCP domains, and no commensurability effect due to thickness is present.

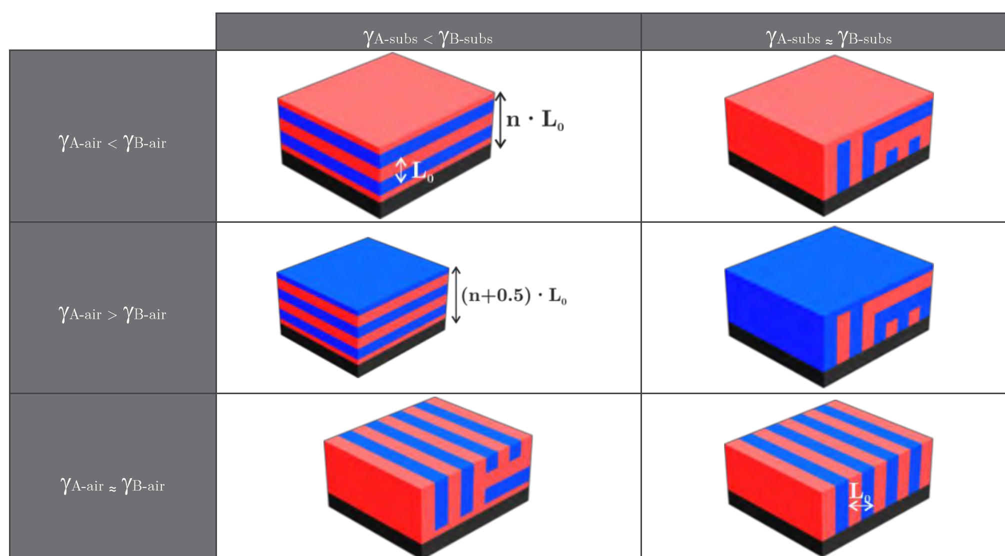

Figure 2.10. Schematic illustrations of a lamellar A-B BCP thin film varying interfacial affinities. $\gamma_{A\text{-sub}}$, $\gamma_{B\text{-sub}}$, $\gamma_{A\text{-air}}$ and $\gamma_{B\text{-air}}$ represent the interfacial energies of A and B with respect to the substrate and air, respectively

As described in Figure 2.11, when BCP do not accomplish the film thickness commensurability condition, because of stretching or compression effects which are energetically unfavorable, BCP tend to mitigate them and fulfill the commensurability condition, by creating some holes or terraces with different number of layers. As it can be observed in the SEM image, in the region where the BCP has a perpendicular orientation, the BCP does not fit the commensurability condition, and therefore it adopts the morphology in which there is no restriction with the film thickness.

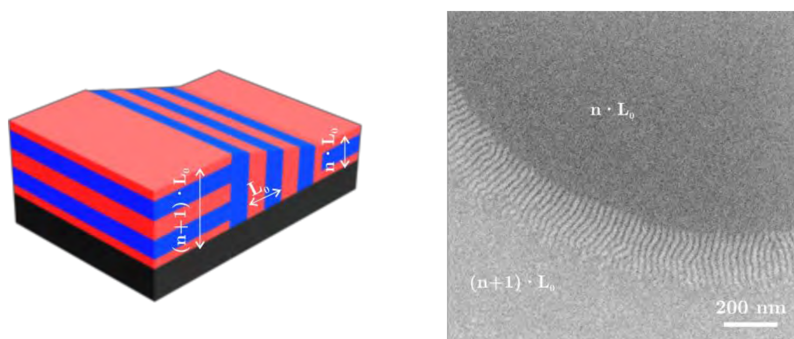

Figure 2.11. Schematics of a lamellar A-B diblock copolymer confined in a system with preferential affinity to red domains on the substrate and air with initial thickness of (n+0.5) · L_0

2.2.4. Interface neutralization

Technological applications require transferring the patterns into a functional material and therefore, there is the need to control the BCP morphology. In general, strong preferential interactions occur between one of the BCP domains and the substrate, which leads to wetting morphologies at the polymer-brush interface. Therefore, the surface has to be able to balance the surface free energies for both BCP domains. This can be overcome by creating a neutral substrate and thus, controlling the interface energies in order to promote the desired morphology. The most used technique to achieve this goal was first introduced by Mansky[34] and it consists in using a *brush polymer* based on the use of random copolymers to induce the perpendicular orientation of BCPs. By properly tuning the brush layer composition, the interface energies can be well controlled and thus, the final BCP morphology.

On the other hand, high-χ BCPs have normally a large surface energy between the two blocks, and this leads to a parallel oriented morphology.[35] Therefore, there has to be a balance between the film thickness, the substrate and the interface energies.[34,36,37] In order to control the interface energy between the air and the BCP and thus its orientation, there are different approaches that be used, including solvent annealing[38,39], electric[40,41] or magnetic[42] fields or the use of top-coats.[6,43] The use of top-coats is more compatible with lithographic processes, but top-coats must be soluble in a solvent that do not disturb the BCP self-assembly.

2.2.5. Thermal and solvent annealing of block copolymer films

As it has been mentioned previously, in order to promote and enhance the ordering of the BCP microdomains it is necessary to introduce some mobility on polymer chains to facilitate the microphase separation process. Furthermore, when using BCP thin films, the molecules are in a non-equilibrium state, trapped on a solvent, and cannot form an ordered large area.[3,44] In order to promote the equilibrium morphology, either thermal treatments or processes in which a solvent vapor is used can be employed.

2.2.5.1. Thermal annealing processes

BCP phase-separation is promoted by the strength of the repulsive interaction between blocks, χN, where χ depends on the temperature as:

$$\chi = \left(\frac{Z}{k_B T}\right)\left[\varepsilon_{AB} - \frac{(\varepsilon_{AA}+\varepsilon_{BB})}{2}\right], \quad (2.3)$$

where Z is the number of nearest neighbors per monomer in the polymer, $k_B T$ is the thermal energy, and $\varepsilon_{AB}, \varepsilon_{AA}, \varepsilon_{BB}$ are the interaction energies between A and B, A and A, and B and B, respectively.

Taking account equation (2.3), χ decreases as function of temperature, but at higher temperatures it is high enough to induce microphase separation. Thermal treatments consist on annealing the BCP above its T_g but below T_{ODT}, in order to increase the mobility of the molecules and promote the microphase separation. These processes are strictly controlled by the BCP film thickness since the compression of polymer chains is energetically unfavorable. Therefore, the microphase separation occurs in the way to reduce the entropic penalty; that is, if the initial film thickness is commensurate with the boundary conditions (see Figure 2.10), then the film is stable and homogeneous. Additionally, in order to minimize the total free energy, the system develops different morphologies. As compared with other processes, thermal treatments are preferred since there is equipment already implemented in industry and there is no waste stream.[44] Nevertheless, thermal treatments are not very effective for some systems which require very long annealing time due to their high T_{ODT}[45] and sometimes they are not suitable for systems which undergo degradation under high temperatures. To address these issues, processes involving the use of a solvent are used.

2.2.5.2. Solvent annealing processes

Solvent vapor annealing processes offer flexibility regarding the choice of the solvent, processing conditions and it permits avoiding the budget temperature that thermal processes involve since the BCP glass transition temperature is decreased by exposing the sample to a vapor.[46,47] In these processes, polymer thin films are exposed to one or more solvents at temperatures below T_g for a period of time to form a swollen and mobile polymer film.[48,49] During the evaporation process, there exists a gradient of solvent concentration which goes from the surface to the inside of the film, thus occurring first the ordering at the film surface.

When solvent annealing processes are used, one has to take into account that the solvent may affect the interaction between BCP domains[50] and polymer interaction with the substrate. The miscibility between a polymer and a solvent is governed by the interaction *polymer-solvent* parameter, χ_{PS}, which can be estimated with the molar volume of the solvent, and the solubility parameters of the solvent and polymer. By using the *Flory-Huggins* interaction criteria, the complete miscibility between polymer and solvent is achieved when $\chi_{PS} < 0.5$, and the affinity between them is stronger when the χ_{PS} value is decreased. Therefore, the selection of a solvent may induce some changes in the degree of microphase separation. On the other hand, it presents a disadvantage in the kinetics when using high-χ BCP systems and therefore, some works have been reported to improve processing time up to some minutes. These results show that a previous heating of the solvent induces a smaller activation energy for the BCP diffusion and thus well-ordered nanostructures can be formed in shorter times.[51,52]

By conveniently combining both processes, highly ordered structures with low defectivity and by using shorter annealing times can be achieved. In this process, known as *solvothermal annealing processes*, the BCP sample is exposed to a solvent vapor and consequently irradiated with microwave energy.[53,54]

2.3. Modelling of block copolymer directed self-assembly

The phase behavior of simple BCPs is understood rather well, although there are some disagreements between theoretical and experimental results.[19,55,56] Therefore, the role of computational modeling consists mainly on exploring parameter variations on the DSA physical mechanism which are difficult to obtain in experiments.

Modelling the DSA process requires a hierarchical approach since polymeric materials exhibit structure on very different scales, ranging from armstrongs to micrometers, and thus the modelling challenge consists in devising models and combining information provided by the different DSA models. It follows that they cannot be included in the same theoretical framework, and different theoretical approaches have been developed depending on the length and time scales.

On the one hand, *atomistic models* provide an accurate prediction of local properties of self-assembled systems with dimensions around 10 nm, and on the other hand, *coarse-grained models* describe the microphase separation in mixed systems by field-theoretic representations of polymer molecules in combination with self-consistent-field calculations on scales in the order of 10 nm to 1 μm.

The atomistic information (statistical segment length, *Flory-Huggins* parameter, the surface energies and the self-diffusion coefficient) is used to parameterize the coarse-grained models, which, in turn, allow predicting the free energy of defects, the DSA kinetics and the mechanisms of defect generation and removal. Then, the information provided by the coarse-grained models can be used to calibrate a reduced model that can be integrated into a lithographic process simulation, by coarse-graining or reverse-mapping the information.

Figure 2.12 shows a schematic representation of the three models as a function of the length and time scale. There is a need of different models and simulation techniques that target properties at different length and time scales, since there is no single model capable of simultaneously extracting all relevant DSA parameters.[57]

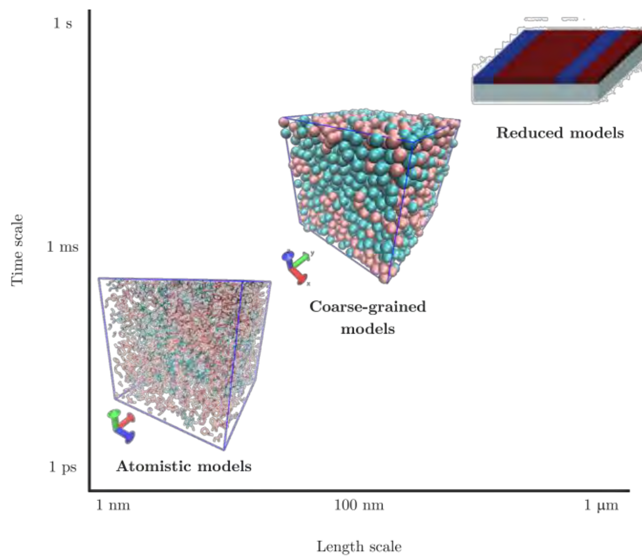

Figure 2.12. Adapted schematic illustration of the different models as a function of time and length scales[58]

2.3.1. Block copolymer kinetics

From the disordered to the ordered state, as the BCP films equilibrate, the individual BCP chains move diffusing through the ever-growing domain interfaces adopting more energetically favorable states. This means that low free-energy defect structures, such as dislocations, can persist but eventually move to the lowest energy state at equilibrium.

Experimentally it is observed that DSA processes induces a diversity of defects which limits the application of BCP DSA into the industry (industry standards require less than 0.01 defects/cm^2).[59] Defects can be conceived as thermal fluctuations in the vicinity of the order-disorder transition where the excess of free energy is comparable to the thermal energy scale, k_BT. Outside the vicinity of the order-disorder transition, where the defect excess of free energy is significantly larger than k_BT, they directly come from the kinetics of structure formation.[60] Additionally to the thermodynamic equilibrium properties, the kinetics of BCP formation is also important since BCPs do not usually form spontaneously long-range-ordered features and they require a thermal or solvent annealing. Therefore, since diffusivity exhibits an Arrhenius dependence (equation (2.4)) annealing times determine the ability of the BCP to eliminate defects.[61] On the other hand, the difference of free energy between the defective and the defect free state is the driver for eliminating defects and it decreases as χN increases.[62] The higher χN the greater is the penalty for mixing in an exponential decrease in diffusion:

$$D = D_0 e^{-0.28(\chi N - 3.5)}, \tag{2.4}$$

where D_0 is the diffusion coefficient of the corresponding non-phase separated polymer.

Equation (2.4) explains why in high-χ BCPs the self-assembly kinetics is very slow (exponential decrease of BCP chain mobility with respect to χN). Therefore, solvent annealing processes are very suitable because they can offer polymer chain mobility at low temperature, thus avoiding the problem of slow self-assembly behavior.

On the other hand, when the BCP self-assemble on a chemical guiding pattern, it can strongly influence the kinetics by modifying the free energy background. The self-assembly kinetics is much slower when the guiding pattern dimensions do not commensurate with L_0, when the chemical interactions between the BCP domains and substrate are weak or when using high density multiplication patterns. Therefore, it is important to understand and control the self-assembly kinetics to annihilate the final trapped defect states, especially observed in line/space patterns. The use of a soft, coarse-grained polymer model is suitable to describe the kinetics of the structure formation since the structure formation evolves in time scales of minutes or hours, but it is, however, non-accessible for atomistic modeling.[63]

2.3.2. Field-theoretic simulations and self-consistent field theory

The coarse-grained model denotes the polymer conformations and their interactions through a coarse-grained bead-spring representation. In this modelling, the atomistic information is used to correlate material properties to the thermodynamics and kinetics of the DSA process.[64,65] Coarse-grained models study complex and three-dimensional DSA processes on the scale of hundreds of nanometers and minutes since the interactions between segments are weak. Small number of atoms are grouped into segments, and then the interactions between these coarse-grained segments are calculated.[57,66,67] These softer interactions arise as a consequence of coarse-graining and can be explained because of the excluded volume interactions, due to the fact that in the microscopic scale atoms cannot overlap (Pauli´s principle).[68,69] Therefore, these soft volume interactions allow for an overlap between the coarse-grained segments.

In the case of a binary blend, the coarse-grained parameters which describe the interactions and correlations on short length scales are, the incompatibility between molecules, χN, the compressibility, κN, the chain dimensions, R_{eo}, and the invariant degree of polymerization, $\bar{N}$, which quantifies the number of neighbors a molecule interacts with:

$$\bar{N} \equiv \left(\frac{\rho_o}{N_{cg}} R_{eo}^3\right)^2, \tag{2.5}$$

where ρ_o is the number density of segments and N_{cg} represents the number of coarse-grained interaction centers. N is a dimensionless parameter and it is smaller than the smallest length scale of physical interest and it is on the range between 16 and 128. χN determines the phase behavior, κN limits the fluctuations of the total density, R_{eo} depicts the length scale, and $\bar{N}$ controls the strength of long wavelength composition fluctuations.[63]

On the other hand, in order to characterize the contact of the DSA domains with the confining boundaries, the surface and interface tensions are used as the coarse-grained invariant parameters. These interactions are represented by convenient force fields and the strength of each of those interactions as depicted in Table 2.1.

Additionally, in order to compute the free energy and the thermodynamic forces that drive the structure formation self-consistent field calculations are used. These calculations are based on a mean-field approximation which allows for the calculation of free energies of self-assembled morphologies.[70]

Table 2.1. Invariant parameters of the coarse-grained model

Interactions	Invariant coarse-grained parameters
Chain connectivity	$\boldsymbol{R_{eo}}$**:** mean squared end-to-end distance of non-interacting polymer coils
	***f*:** fraction of polymer domains
Polymer melt	$\boldsymbol{\kappa N}$**:** isothermal liquid compressibility · Invariant degree of polymerization
Repulsion between unlike species	$\boldsymbol{\chi N}$**:** Flory Huggins parameter · Invariant degree of polymerization
Interaction of the domains with the guiding pattern	Geometry of confinement (measured in units of R_{eo} or L_o)
	$\boldsymbol{\gamma_{SA}}$, $\boldsymbol{\gamma_{SB}}$**:** Surface free-energies of the segments species with the confining boundaries
Dynamics of macromolecules	***D*:** Self-diffusion coefficient which defines time scale

These particle-based models described before provide detailed information of the macromolecular conformations, but they are too expensive to explore the DSA on large-scale lithographic processes. Therefore, new reduced models are being studied since they can be integrated into a lithographical process flow: *Continuum models*[71–73] and *interface Hamiltonians.*[74,75] On the one hand, continuum models describe DSA processes by collective variables in space and time in order to predict the three-dimensional BCP structure, and they can be derived from the SCFT in the WSL between domains. On the other hand, interface Hamiltonians describe the DSA process by only the evolution of the interfaces between the copolymer domains, and they provide an appropriate description on the SSL. They overcome the limitations of continuum models in dealing with the disparity between interfaces, although it is difficult to derive these interactions in complex geometries

2.4. High-chi block copolymers

Currently, microelectronics industry is demanding the development of new methods focused on the production of ever-smaller structures. DSA is an alternative technique which provides a complementary solution to the resolution limitation of conventional lithography. PS-*b*-PMMA has been the most studied BCP system, principally due to the fact that both PS and PMMA have almost equal surface energies which allows forming morphological and

uniform patterns all the way through the film.[34] On the other hand, PMMA can be easily etched by O_2 plasma or UV exposure, and then the remaining material can be used as a mask for pattern transfer.[76,77] Moreover, new techniques based on using SIS have been recently reported showing very high aspect ratio structures after pattern transfer, due to the fact of an enhancement on the etch selectivity between PS and PMMA.[78–80]

As discussed previously, when the enthalpic contributions are sufficiently large to overcome the entropy to mix the blocks, the microphase segregations occurs originating different nanostructures depending on the relative volume fraction of the two blocks. For lamellar block copolymer (f = 0.5), this condition occurs when the product χN is above 10.5, which means that every BCP has a minimum achievable size.[3,19] Therefore, in order to obtain smaller features, the degree of polymerization, N, has to be reduced since it reduces the characteristic BCP length scale, and the χ value has to be increased to balance the product χN and keep constant the level of phase segregation. In that sense, since PS-*b*-PMMA has a low χ value (0.041 at 25°C)[18] which limits the minimum feature size around 12 nm, and therefore, restricting its utility for the next generation nodes.[6,38,81] Therefore, in order to achieve smaller domains, a BCP with larger interaction parameter has to be used. Nevertheless, the design of high-χ systems which provide sub-20 nm resolution have to be demonstrated with a controlled BCP synthesis and with a good etching selectivity.

The generation of high-χ BCP systems can be performed by introducing polymer domains which have stronger interactions among identical monomers and high incompatibility among different domains. Normally it can be achieved by introducing very highly polar groups, fluorine or silicon-rich blocks.

2.4.1. Organic based high-χ block copolymers

Organic based BCP usually present low χ values. Moreover, these BCP share similar chemistries which translates in a low etching contrast between blocks, and consequently low aspect ratio features.[82] An example of organic high-χ BCP system is poly(styrene-*b*-D,L-lactide), PS-*b*-PLA, with both hydrophobic (PS) and hydrophilic (PLA) domains. This amphiphilic nature gives rise to a χ value of 0.23.[83] Other organic high-χ BCP are depicted in Table 2.2.

However, such materials are generally difficult to generate due to their dissimilar polarities and properties between blocks. This means that they cannot easily show the perpendicular morphology with a thermal annealing as does PS-*b*-PMMA, and they need either a solvent annealing or an additional top-coat layer.

2.4.2. Inorganic based high-χ block copolymers

Inorganic based BCP are being intensively studied due to the high etching contrast between domains. They are normally formed by one organic domain and one inorganic

block which is resistant to oxygen plasma. The inorganic part is normally a silicon or iron containing domain which forms the corresponding oxide after O_2 plasma exposure and retains the pattern from the original features. The first polymer used was polydimethylsiloxane (PDMS)-containing BCP with a backbone formed by Si-O bonds.[84]

The highest-χ BCP system synthesized so far, is an ABA triblock copolymer containing PLA and PDMS end and midblock, respectively.[85] These domains are extremely incompatible ($\chi = 1.4$) and PDMS provides a high etch resistivity, while PLA is almost twice as susceptible to be etched compared to PS. Other inorganic high-χ systems are summarized in Table 2.2.

Table 2.2. Organic and inorganic high-χ BCP systems collected from several works at 25°C

Organic BCPs		Inorganic BCPs	
BCP system	**χ value**	**BCP system**	**χ value**
PS-*b*-PMMA	0.041[18]	PS-*b*-PFS	0.08[34]
PS-*b*-PEO	0.077[86]	PS-*b*-PDMS	0.26[84]
PS-*b*-P2VP	0.178[87]	PTMSS-*b*-PLA	0.46[39]
PS-*b*-PLA	0.233[83]	PS-*b*-MH	0.58[88]
PS-*b*-PI	0.110[89]	PLA-*b*-PDMS-*b*-PLA	1.4[85]

There are other high-χ systems which combine block copolymers with inorganic species to form an hybrid material.[90] *Park et al.* describe a system consisting of a mixture of poly(styrene-*b*-ethylene oxide), PS-*b*-PEO, and a low molecular weight organosilicate forming 7 nm pitch lamellae morphology. On the other hand, there are other examples in which a metal salt is selectively added to a PS-*b*-PEO, reducing its size to 3 nm.[91] Nevertheless, the fact of adding a metal salt can bring complications during the processing steps.

Once the basis of BCP chemistry and physics has been studied, in the next chapters the different chemical and graphoepitaxy processes developed and optimized at IMB-CNM will be described. These processes will be implemented for both PS-*b*-PMMA and high-χ materials. All these results, lead to go step further and implement the chemical epitaxy process at larger scale in the cleanroom of CEA-Leti which operates with a wafer scale of 300 mm. Moreover, the role of the chemical interactions which take place between the guiding pattern and the BCP domains will be experimentally characterized and modelled.

2.5. References

1. Jenkins, A. D., *et al.* Glossary of Basic Terms in Polymer. *Pure Appl. Chem.* **68,** 2287–2311 (1996).

2. Hamley, I. W. *The physics of block copolymers.* (Oxford University Press, 1998).

3. Bates, F. S. *et al.* Block copolymer thermodynamics: theory and experiment. *Annu. Rev. Phys. Chem.* **41,** 525–557 (1990).

4. Park, C., *et al.* Enabling nanotechnology with self assembled block copolymer patterns. *Polymer.* **44,** 6725–6760 (2003).

5. Segalman, R. Patterning with block copolymer thin films. *Mater. Sci. Eng. R Reports* **48,** 191–226 (2005).

6. Bates, C. M. *et al.* Polarity-switching top coats enable orientation of sub-10-nm block copolymer domains. *Science* **338,** 775–9 (2012).

7. Moad, G. *et al. The Chemistry of Radical Polymerization.* (2006).

8. Solomon, D. H., *et al.* Polymerization process and polymers produced thereby. (1986).

9. Kato, M., *et al.* Polymerization of Methyl Methacrylate with the Carbon Tetrachloridel Dichlorotris- (triphenylphosphine)ruthedum(II)/Methylaluminum Bis(2,6-di-tert-butylphenoxide) Initiating System: Possibility of Living Radical Polymerization1. *Macromolecules* **28,** 1721–1723 (1996).

10. Wang, J. S. *et al.* Controlled 'living' radical polymerization. Atom transfer radical polymerization in the presence of transition-metal complexes. *J. Am. Chem. Soc.* **117,** 5614–5615 (1995).

11. Le, T. P., *et al.* Polymerization with living characteristics. (1998).

12. Chiefari, J. *et al.* Living Free-Radical Polymerization by Reversible Addition - Fragmentation Chain Transfer : The RAFT Process We wish to report a new living free-radical polymer- ization of exceptional effectiveness and versatility, *Macromolecules* **31,** 5559–5562 (1998).

13. Rizzardo, E. *et al.* Tailored polymers by free radical processes. *Macromol. Symp.* **143,** 291–307 (1999).

14. Chiefari, J. *et al. Handbook of radical polymerization.* (John Wiley & Sons, 2002).

15. Moad, G., *et al.* Living radical polymerization by the RAFT process. *Aust. J. Chem.* **58,** 379–410 (2005).

16. Perrier, S. *et al.* Macromolecular design via reversible addition-fragmentation chain transfer (RAFT)/xanthates (MADIX) polymerization. *J. Polym. Sci. Part A Polym. Chem.* **43,** 5347–5393 (2005).

17. Flory, P. J. *Principles of Polymer Chemistry.* (1953).

18. Russell, T. P. Temperature Dependence of the Interaction Parameter of Polystyrene and Poly (methyl methacrylate). *Macromolecules* 890–893 (1990).

19. Leibler, L. Theory of microphase separation in block copolymers. *Macromolecules* **13,** 1602–1617 (1980).

20. Meier, D. J. Theory of Block Copolymers. I. Domain Formation in A-B Block Copolymers. *J. Polym. Sci. Part C* **26,** 81–98 (1969).

21. Helfand, E. Block Copolymer Theory. III. Statistical Mechanics of the Microdomain Structure. *Macromolecules* **8,** 552–556 (1975).

22. Fredrickson, G. H. *et al.* Fluctuation effects in the theory of microphase separation in block copolymers. *J. Chem. Phys.* **87,** 697 (1987).

23. Bates, F. S. Polymer-Polymer Phase Behavior. *Science.* **251,** (1990).

24. Bates, F. S. *et al.* Fluctuations, Conformational Asymmetry and Block Copolymer Phase Behaviour. *Faraday Discuss.* **98,** 7–18 (1994).

25. Vavasour, J. D. *et al.* Self-consistent mean field theory of the microphase diagram of block copolymer/neutral solvent blends. *Macromolecules* **25,** 2041–2045 (1992).

26. Matsen, M. W. *et al.* Stable and unstable phases of a diblock copolymer melt. *Phys. Rev. Lett.* **72,** 2660–2663 (1994).

27. Matsen, M. W. *et al.* Unifying Weak- and Strong-Segregation Block Copolymer Theories. *Macromolecules* **29,** 1091–1098 (1996).

28. Matsen, M. W. Effect of architecture on the phase behavior of AB-type block copolymer melts. *Macromolecules* **45,** 2161–2165 (2012).

29. Tyler, C. A. *et al.* Orthorhombic Fddd network in triblock and diblock copolymer melts. *Phys. Rev. Lett.* **94,** 1–4 (2005).

30. Bailey, T. S., *et al.* A noncubic triply periodic network morphology in poly(isoprene-b-styrene-b-ethylene oxide) triblock copolymers. *Macromolecules* **35,** 7007–7017 (2002).

31. Kim, M. I. *et al.* Stability of the Fddd phase in diblock copolymer melts. *Macromolecules* **41,** 7667–7670 (2008).

32. Im Kim, M. *et al.* Determination of the FDDD phase boundary in polystyrene-block-polyisoprene diblock copolymer melts. *Macromolecules* **42,** 5266–5271 (2009).

33. Takenaka, M. *et al.* Directed self-assembly of block copolymers. *Curr. Opin. Chem. Eng.* **2,** 88–94 (2013).

34. Mansky, P. Controlling Polymer-Surface Interactions with Random Copolymer Brushes. *Science.* **275,** 1458–1460 (1997).

35. Maher, M. J. *et al.* Interfacial design for block copolymer thin films. *Chem. Mater.* **26,** 1471–1479 (2014).

36. Huang, E., *et al. N*eutrality conditions for block copolymer systems on random copolymer brush surfaces. *Macromolecules* **32,** 5299–5303 (1999).

37. Hur, S.-T., *et al.* H. Investigation for correlation between elastic constant and thermal stability of liquid crystalline blue phase I. *Soft Matter* **7,** 8800 (2011).

38. Cushen, J. D. *et al.* Oligosaccharide/silicon-containing block copolymers with 5 nm features for lithographic applications. *ACS Nano* **6,** 3424–3433 (2012).

39. Cushen, J. D. *et al.* Thin Film Self-Assembly of Poly(trimethylsilylstyrene- b - d , l - lactide) with Sub-10 nm Domains. *Macromolecules* **45,** 8722–8728 (2012).

40. Boker, A. *et al.* Large scale domain alignment of a block copolymer from solution using electric fields. *Macromolecules* **35,** 1319–1325 (2002).

41. Olszowka, V. *et al.* Electric field alignment of a block copolymer nanopattern: direct observation of the microscopic mechanism. *ACS Nano* **3,** 1091–1096 (2009).

42. Gopinadhan, M. *et al.* Thermally switchable aligned nanopores by magnetic-field directed self-assembly of block copolymers. *Adv. Mater.* **26,** 5148–5154 (2014).

43. Maher, M. J. *et al.* Directed Self-Assembly of Silicon-Containing Block Copolymer Thin Films. *ACS Appl. Mater. Interfaces* **7,** 3323–3328 (2015).

44. Bates, C. M., *et al.* Block copolymer lithography. *Macromolecules* **47,** 2–12 (2014).

45. Han, E. *et al.* Perpendicular Orientation of Domains in Cylinder-Forming Block Copolymer Thick Films by Controlled Interfacial Interactions. *Macromolecules* **42,** 4896–4901 (2009).

46. Bang, J. *et al.* Defect-free nanoporous thin films from ABC triblock copolymers. *J. Am. Chem. Soc.* **128,** 7622–7629 (2006).

47. Jeong, J. W., *et al.* Highly Tunable Self-Assembled Nanostructures from a Poly(2-vinylpyridine-b-dimethylsiloxane) Block Copolymer. *Nano Lett.* **11,** 4095–4101 (2011).

48. Sinturel, C., *et al.* Solvent vapor annealing of block polymer thin films. *Macromolecules* **46,** 5399–5415 (2013).

49. Park, W. I. *et al.* Tunable and rapid self-assembly of block copolymers using mixed solvent vapors. *Nanoscale* **6,** 15216–21 (2014).

50. Yu, X. *et al.* Morphology development of ultrathin symmetric diblock copolymer film via solvent vapor treatment. *Macromolecules* **37,** 7301–7307 (2004).

51. Lodge, T. P. *et al.* Mechanisms of chain diffusion in lamellar block copolymers. **75,** 657–660 (1995).

52. Ruiz, R., *et al.* Effect of structural anisotropy on the coarsening kinetics of diblock copolymer striped patterns. *Phys. Rev. B - Condens. Matter Mater. Phys.* **77,** 1–5 (2008).

53. Zhang, X., *et al.* Fast assembly of ordered block copolymer nanostructures through microwave annealing. *ACS Nano* **4,** 7021–7029 (2010).

54. Gotrik, K. W. *et al.* Solvothermal annealing of block copolymer thin films. *Nano Lett.* **13,** 5117–5122 (2013).

55. Semenov, A. N. Contribution to the theory of microphase layering in block-copolymer melts. **1256,** 733–742 (1985).

56. Fredrickson, G. H. Dynamics and rheology of inhomogeneous polymeric fluids: A complex Langevin approach. *J. Chem. Phys.* **117,** 6810–6820 (2002).

57. Praprotnik, M., *et al.* Multiscale simulation of soft matter: from scale bridging to adaptive resolution. *Annu. Rev. Phys. Chem.* **59,** 545–571 (2008).

58. Computational Lithography for directed Self Assembly: Materials, Models and Processes (CoLiSA: 619793). European Union Seventh Framework Programme

59. Jeong, S. J., *et al.* Directed self-assembly of block copolymers for next generation nanolithography. *Mater. Today* **16,** 468–476 (2013).

60. Li, W. *et al.* Defects in the Self-Assembly of Block Copolymers and Their Relevance for Directed Self-Assembly. 187–218 (2015).

61. Takahashi, H. *et al.* Defectivity in laterally confined lamella-forming diblock copolymers: Thermodynamic and kinetic aspects. *Macromolecules* **45,** 6253–6265 (2012).

62. Peters, A. J., *et al.* Understanding defects in DSA: calculation of free energies of block copolymer DSA systems via thermodynamic integration of a mesoscale block-copolymer model. **9049,** 90492E (2014).

63. Daoulas, K. C., *et al.* Morphology of multi-component polymer systems: single chain in mean field simulation studies. *Soft Matter* **2,** 573 (2006).

64. Stoykovich, M. P. *et al.* Directed Self-Assembly of Block Copolymers for Nanolithography : Essential Integrated Circuit Geometries. **1,** 168–175 (2007).

65. Müller, M. Geometry-controlled interface localization-delocalization transition in block copolymers. *Phys. Rev. Lett.* **109,** 1–5 (2012).

66. Baschnagel, J. *et al.* Computer simulations of polymers close to solid interfaces: Some selected topics. *Interface Sci.* **11,** 159–173 (2003).

67. Mullinax, J. W. *et al.* Generalized Yvon-Born-Green Theory for Molecular Systems. *Phys. Rev. Lett.* **103,** 1–4 (2009).

68. Noid, W. G. *et al.* The multiscale coarse-graining method. I. A rigorous bridge between atomistic and coarse-grained models. *J. Chem. Phys.* **128,** 1–11 (2008).

69. Editor, G. *et al.* This paper is published as part of a PCCP Themed Issue on : Coarse-grained modeling of soft condensed matter. (2009)

70. Matsen, M. W. The standard Gaussian model for block copolymer melts. *J. Phys. Condens. Matter* **14,** 21–47 (2002).

71. Petera, D. *et al.* Effect of patterned surface on diblock-copolymer melts and polymer blends near the critical point. *J. Chem. Phys.* **107,** 9640 (1997).

72. Chen, H. *et al.* Morphology of thin block copolymer films on chemically patterned substrates. *J. Chem. Phys.* **108,** 6897 (1998).

73. Tsori, Y. *et al.* Diblock Copolymer Ordering Induced by Patterned Surfaces above the Order - Disorder Transition. 2719–2727 (2001).

74. Wang, Q., *et al.* Symmetric diblock copolymer thin films confined between homogeneous and patterned surfaces: Simulations and theory. *J. Chem. Phys.* **112,** 9996–10010 (2000).

75. Edwards, E. W., *et al.* Precise control over molecular dimensions of block-copolymer domains using the interfacial energy of chemically nanopatterned substrates. *Adv. Mater.* **16,** 1315–1319 (2004).

76. Stuen, K. O., *et al.* Dimensional scaling of cylinders in thin films of block copolymer-Homopolymer ternary blends. *Macromolecules* **42,** 5139–5145 (2009).

77. Ruiz, R. *et al.* Density Multiplication and Improved Copolymer Assembly. *Science.* **321,** 936–940 (2008).

78. Peng, Q., *et al.* Nanoscopic patterned materials with tunable dimensions via atomic layer deposition on block copolymers. *Adv. Mater.* **22,** 5129–5133 (2010).

79. Peng, Q., *et al.* A route to nanoscopic materials via sequential infiltration synthesis on block copolymer templates. *ACS Nano* **5,** 4600–4606 (2011).

80. Moon, H. S. *et al.* Atomic layer deposition assisted pattern multiplication of block copolymer lithography for 5 nm scale nanopatterning. *Adv. Funct. Mater.* **24,** 4343–4348 (2014).

81. Yue, Z., *et al.* SAXS analysis of the Order-disorder transition and the interaction parameter of Polystyrene-block-poIy(methyl methacrylate). *Macromolecules* **41,** 9948–9951 (2008).

82. Delcambre, *et al.* Mechanical properties of antiplasticized polymer nanostructures. *Soft Matter* **6,** 2475 (2010).

83. Keen, I. *et al.* Control of the Orientation of Symmetric Poly(styrene)-block-poly(D,L-lactide) (2012).

84. Hartney, M. A., *et al.* Block copolymers as bilevel resists. *J. Vac. Sci. Technol. B J. Chem. Phys.* **3,** 1346–1241 (1985).

85. Rodwogin, *et al.* Polylactide-poly(dimethylsiloxane)-polylactide triblock copolymers as multifunctional materials for nanolithographic applications. *ACS Nano* **4,** 725–732 (2010).

86. Frielinghaus, H. *et al.* Micro - vs . macro-phase separation in binary blends of poly (styrene)-poly(isoprene) and poly(isoprene)-poly(ethylene oxide) diblock copolymers. *Eur. Lett.* **53,** 680–686 (2001).

87. Dai, K. H. *et al.* Determining the temperature-dependent Flory interaction parameter for strongly immiscible polymers from block copolymer segregation measurements. *Polymer.* **35,** 157–161 (1994).

88. Otsuka, I. *et al.* Control of 10 nm scale cylinder orientation in self-organized sugar-based block copolymer thin films. *Nanoscale* **5,** 2637–41 (2013).

89. Lecommandoux, S. *et al.* Microphase Separation of Linear and Cyclic Block Copolymers Poly(styrene-b-isoprene): SAXS Experiments. *Macromolecules* **37,** 1843–1848 (2004).

90. Park, S.-M., *et al.* Patterning sub-10 nm line patterns from a block copolymer hybrid. *Nanotechnology* **19,** 455304 (2008).

91. Park, S. *et al.* Macroscopic 10-terabit-per-square-inch arrays from block copolymers with lateral order. *Science* **323,** 1030–1033 (2009).

92. Moore, G. E. Cramming more components onto integrated circuits. **38,** (1975).

93. Jan, C. H. *et al.* A 22nm SoC platform technology featuring 3-D tri-gate and high-k/metal gate, optimized for ultra low power, high performance and high density SoC applications. *Electron Devices Meet. IEDM* 44–47 (2012).

94. Neisser, M. *et al.* ITRS lithography roadmap: 2015 challenges. *Adv. Opt. Technol.* **4,** 235–240 (2015).

95. Liu, G., *et al.* Integration of Density Multiplication in the Formation of Device-Oriented Structures by Directed Assembly of Block Copolymer-Homopolymer Blends. *Adv. Funct. Mater.* **20,** 1251–1257 (2010).

96. Rathsack, B. *et al.* Advances in directed self assembly integration and manufacturability at 300 mm. **8682,** 86820K (2013).

97. Hinsberg, W., *et al.* Self-Assembling Materials for Lithographic Patterning: Overview, Status and Moving Forward. *Proc. SPIE* **7637,** 76370G–76370G–11 (2010).

98. Rincon Delgadillo, P. *et al.* Defect source analysis of directed self-assembly process (DSA of DSA). *Proc. SPIE* **8680,** 86800L–86800L–9 (2013).

99. Gronheid, R. *et al.* Defect reduction and defect stability in IMEC's 14nm half-pitch chemo-epitaxy DSA flow. **9049,** 904905 (2014).

100. Somervell, M. *et al.* Driving DSA into Volume Manufacturing. **9425,** 1–11 (2015).

101. Tiron, R. *et al.* Pattern density multiplication by direct self assembly of block copolymers: toward 300mm CMOS requirements. *Proc. SPIE* **8323,** 83230O–83230O–7 (2012).

102. Tada, Y. *et al.* Directed Self-Assembly of Diblock Copolymer Thin Films on Chemically-Patterned Substrates for Defect-Free Nano-Patterning. *Macromolecules* **41,** 9267–9276 (2008).

103. Kim, S. O. *et al.* Epitaxial self-assembly of block copolymers on lithographically defined nanopatterned substrates. 411–414 (2003).

104. Edwards, E. W., *et al.* Long-Range Order and Orientation of Cylinder-Forming Block Copolymers on Chemically Nanopatterned Striped Surfaces. 3598–3607 (2006).

105. Stoykovich, M. P. *et al.* Directed Assembly of Block Copolymer Blends into Nonregular Device-Oriented Structures. **1442,** (2014).